

國立交通大學
材料科學與工程研究所
博士論文

化學氣相沈積法奈米碳管之製作與特性研究

Synthesis and Characterization of Chemical Vapor
Deposition Carbon Nanotubes



研究生：林建良

指導教授：陳家富 博士

中華民國九十三年六月

化學氣相沈積法奈米碳管之製作與特性研究

Synthesis and Characterization of Chemical Vapor Deposition Carbon Nanotubes

研究生：林建良
指導教授：陳家富 博士

Student : Chien-Liang Lin
Advisor : Dr. Chia-Fu Chen

國立交通大學

材料科學與工程研究所



Submitted to Department of material Science and Engineering

College of Engineering

National Chiao Tung University

In partial Fulfillment of the Requirements

For the Degree of Doctor of Philosophy

In Material Science and Engineering

June 2004

Hsinchu, Taiwan, Republic of China

中華民國九十三年六月

化學氣相沈積法奈米碳管之製作與特性研究

研究生：林建良

指導教授：陳家富

國立交通大學材料科學與工程研究所 博士班

摘要

本論文最大的成就在於提出一個直接成長多層壁奈米碳管的簡易方法，稱之為熱絲化學氣相沈積法。此合成裝置類似用於成長鑽石的熱電子(或稱熱燈絲)化學氣相沈積法，其不同於鑽石成長之裝置設計在於燈絲部分以 Fe-Cr 線替代 W 線，目的在於利用 Fe-Cr 線加熱時，其溫度接近其融點 (約 1520 °C) 附近所蒸發出來之 Fe、Cr 元素作為成長碳管之觸媒。其成長方法是以 CO₂ 或 Ar 當作載氣通過酒精送入反應區，即可將各種不同的不規則捲曲碳管及直立碳管直接成長於矽晶片。實驗結果顯示，當 CO₂ 載氣的流動方向垂直接向於試片時，試片上會長出直徑 60-80 nm 的不規則捲曲碳管；當載氣平行流過試片表面時，則生成直徑約為 10 nm 的直立碳管。不規則捲曲碳管為多層壁且為竹節狀，直立碳管則為多層壁但無竹節出現。綜合兩種碳管的頂端並沒有觸媒出現，推測碳管是屬於底端成長模式。以熱絲法直接成長的直立奈米碳管，起始電場為 1.1 V/μm (10 μA/cm² 時)，場發射電流密度為 0.54 mA/cm² (2 V/μm 時)。

另外，本論文也嘗試使用微波電漿化學氣相沈積法，以 CH₄/CO₂ 氣體系，及用基材自我供應觸媒方式來成長奈米碳管，探討比較兩種方式所成長碳管之成長機構與特性差異。熱絲化學氣相沈積法中用 Fe-Cr 線 (71.4 wt % Fe 及 22.5 wt % Cr) 做為觸媒來源，在此則用不鏽鋼 304 (70 wt % Fe、19 wt % Cr 及 9 wt % Ni) 當作基材來成長奈米碳管。結果顯示準直性佳的碳管可直接生成，然而基材中重要的 Cr 成分，並沒有出現於碳管頂端的觸媒顆粒。故為瞭解 Cr 對成長奈米碳管的特性，用 CH₄/H₂ 及 CH₄/CO₂ 這兩種氣體系在 Cr 膜上成長碳管。當以 CH₄/CO₂ 為反應氣體時，實驗中並未有明顯的碳管生成。

當以 CH_4/H_2 為反應氣體時，則先用施加負偏壓的 H_2 電漿進行 Cr 膜的前處理，依前處理時間的長短，造成 Cr 膜不同的表面型態，然後再加入 CH_4 （碳源）進行奈米碳管的成長。實驗證明 Cr 膜也能成長奈米碳管，但只限制在 5 分鐘前處理的 Cr 膜上；意即 Cr 膜只有在特定的表面型態時，才具有生成奈米碳管的觸媒作用。總結本論文在微波電漿化學氣相沈積法所成長出的碳管，成長過程皆符合頂端成長模式。

比較熱絲化學氣相沈積法與微波電漿化學氣相沈積法，熱絲化學氣相沈積法結合物理及化學氣相沈積法，具有便宜、大面積且連續合成奈米碳管的潛力。同時也不需要真空的環境下進行。微波電漿化學氣相沈積法則可生成分佈密度較高且較均勻的奈米碳管。場發射性質則以熱絲化學氣相沈積法所長出的直立碳管最佳，推論是由於其直立性、適中的碳管分佈密度、碳管表面覆蓋的非晶質碳，以及極細的碳管管徑所造成的。



Synthesis and Characterization of Chemical Vapor Deposition

Carbon Nanotubes

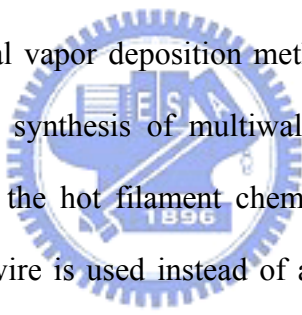
Student : Chien-Liang Lin

Advisor : Dr. Chia-Fu Chen

Institute of Material Science and Engineering

National Chiao Tung University

Abstract



A direct hot wire chemical vapor deposition method, which is the main feature of this thesis, is proposed for *in situ* synthesis of multiwalled carbon nanotubes. This synthesis apparatus is similar to that in the hot filament chemical vapor deposition used to deposit diamonds. However, a Fe-Cr wire is used instead of a W wire in synthesizing diamonds to grow nanotubes. Fe-Cr wires need to be heated to 1200 °C, approaching the melting point (~1520 °C) of itself. Evaporated metal atoms, Fe and Cr, can be considered to catalyze the growth of carbon nanotubes. Different morphologies of carbon nanotubes, curved or aligned, were deposited directly on the Si substrate with CO₂ or Ar as the carrier gas through alcohol. Indicated in the experimental results are that the vertical flow direction of CO₂ to the substrate produced the random network of curved carbon nanotubes with the diameter of 60-80 nm. In contrast, horizontal flow direction of CO₂ to the substrate produced the aligned carbon nanotubes of about 10 nm in diameter. The HRTEM observation tells that curved nanotubes were multiwalled and bamboo-like in structure; while vertical nanotubes multiwalled but without bamboo-like structure. In both cases, there was no catalyst in the top end of nanotubes. Therefore, the growth mechanism is suggested to be base-growth model. The

turn-on field of the aligned carbon nanotubes was $1.1 \text{ V}/\mu\text{m}$ (at $10 \mu\text{A}/\text{cm}^2$), and the emission current density $0.54 \text{ mA}/\text{cm}^2$ (at $2 \text{ V}/\mu\text{m}$).

Meanwhile, microwave plasma chemical vapor deposition by using CH_4/CO_2 gas mixture was used to grow CNTs directly on substrates, which were self-catalyzed, for comparisons of the growth mechanism and characterizations of carbon nanotubes grown by these two deposition system. In the hot wire chemical vapor deposition, CNTs were grown by Fe-Cr wires (Fe: 71.4 wt %, Cr: 22.5 wt %) that act as catalyst sources. Therefore, typical stainless steel 304 (Fe: 70 wt %, Cr: 19 wt %, Ni: 9 wt %) was used as the substrate to grow CNTs in this system. Experimental results show that well-aligned carbon nanotubes can grow directly on the stainless steel. However, the metal catalysts on the top of the carbon nanotubes contain Fe and Ni, but no Cr. To realize the characterization of Cr, carbon nanotubes were attempted to grow on a Cr film by using CH_4/H_2 or CH_4/CO_2 gas mixture. The CH_4/CO_2 mixture produced no obvious nanotubes under these conditions, but for CH_4/H_2 source gas, bias-enhanced H_2 plasma pretreatment was performed for various periods to modify the surface of the Cr film, then CH_4 (carbon source) was added for growth of carbon nanotubes. Experimental results show that carbon nanotubes can be grown, but just in a narrow Cr surface condition. A summation of the studies in microwave plasma chemical vapor deposition suggests the growth mechanism to be tip-growth model.

Revealed in the comparison of these two methods is the superior potential of the hot wire chemical vapor deposition for the inexpensive and continuous mass synthesis of nanotubes by combining both physical and chemical vapor depositions. Besides, hot wire chemical vapor deposition is not necessary to operate under vacuum. Microwave plasma chemical vapor deposition can yield CNTs with higher density and uniformity in this stage. In these studies, vertical CNTs grown by hot wire chemical vapor deposition possess the best field emission properties. It may be due to the alignment of MWCNT, medium density, ta-c coated, and the small diameter to enhance their field emission properties.

誌 謝

感謝國立交通大學所有教導過我的老師，尤其是我的指導教授－陳家富老師。打從交大材料所創所時期開始，在碩士班就接受陳老師的指導。工作多年後，重返校園追求更高的學識，陳老師是我不變的選擇。謝謝他在論文研究上的指導與鼓勵，使得這篇論文能順利完成。更重要的是陳老師對學生的照顧與愛護。

口試時承蒙郭正次老師、陳三元老師、施漢章老師、薛富盛老師、賴宏仁老師、林啟瑞老師、林麗瓊老師的指導及寶貴意見，在此亦由衷的表示感謝。

感謝學弟王滋銘與陳建銘協助實驗的完成。也感謝林琨程、李延煒、陳密、蔡佳倫、施士塵、陳光中、陳建仲等在實驗上提供意見及討論。以前工作上的好同事，鄭耀宗博士及林修正博士也提供不少的建議及指教。此外，合晶科技提供實驗用的矽晶片，也值得感謝。

最後，感謝我的老婆素蕙，這些年來對我全力的支持，以及女兒小葳，讓我能同時兼顧博士課程以及論文的研究，無後顧之憂。僅以此論文獻給我最親愛的家人。

讀博士班這五年來，有著無數人的幫助。要謝的人太多了，只能再說一次感恩啦。

Contents

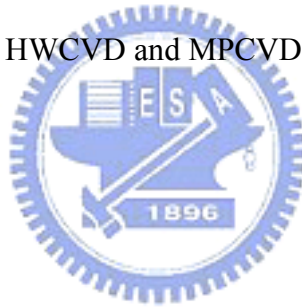
ABSTRACT (in Chinese)	I
ABSTRACT (in English)	III
ACKNOWLEDGEMENTS (in Chinese)	V
CONTENTS	VI
LIST OF TABLES	IX
LIST OF FIGURES	X
1 INTRODUCTION	1
1.1 Background	1
1.2 Motivation and Objectives	2
1.3 Outline of this Thesis	3
2 LITERATURE REVIEW	4
2.1 Basic Knowledge of Carbon Materials	4
2.1.1 Fullerenes	6
2.1.2 Carbon Nanofibers	7
2.2 Structure and Properties of Carbon Nanotubes	8
2.2.1 Structure	8
2.2.2 Properties	11
2.3 Carbon Nanotube Synthesis	14
2.3.1 Arc Discharge	14
2.3.2 Laser Ablation	15
2.3.3 Catalytically Chemical Vapor Deposition (CVD)	16
2.4 Catalytic Growth Mechanisms of Carbon Nanotubes	20
2.5 Field Emission	22
2.5.1 Field Emission from Carbon Nanotube Films	22

2.5.2	Field Emission Applications of Carbon Nanotube Films	29
3	EXPERIMENTAL DETAILS	36
3.1	HWCVD	36
3.1.1	Deposition System	36
3.1.2	Depositing Conditions	37
3.2	MPCVD	38
3.2.1	Deposition System	38
3.2.2	Carbon Nanotubes Grown on AISI 304	40
3.2.3	Carbon Nanotubes Grown on Cr Film	40
3.3	Characterization of Carbon Nanotubes	41
3.3.1	Scanning Electron Microscopy (SEM)	41
3.3.2	Micro-Raman Spectroscopy	41
3.3.3	Atomic Force Microscopy (AFM)	42
3.3.4	High Resolution Transmission Electron Microscopy (HRTEM)	42
3.3.5	I-V Measurement	42
4	RESULTS AND DISCUSSION	44
4.1	Carbon Nanotubes <i>In Situ</i> Grown on Silicon by Using HWCVD	44
4.1.1	Background	44
4.1.2	Characterization of Carbon Nanotubes	45
4.1.3	Effect of Carrier Gases and Flow Rate on Growth of CNTs	48
4.1.4	Effect of Carrier Gas Flow Direction on Growth of CNTs	54
4.1.5	Field Emission Properties	60
4.2	Growth Model of Carbon Nanotubes by Using HWCVD	62
4.3	Carbon Nanotubes Grown on AISI 304 by Using MPCVD: CH ₄ /CO ₂	
Reactant Gas		69
4.3.1	Background	69

4.3.2 Effect of Bias on Growth of CNTs	70
4.3.3 Various Periods of Growth of CNTs	72
4.3.4 Catalytic Effect of Metal	80
4.3.5 Field Emission Properties	82
4.4 Carbon Material Grown on Cr Film by Using MPCVD: CH ₄ /CO ₂ Reactant Gas	83
4.4.1 Background	83
4.4.2 Characterization of Carbon Material	83
4.4.3 Field Emission Properties	85
4.5 Carbon Nanotubes Grown on Cr Film by Using MPCVD: CH ₄ /H ₂ Reactant Gas	88
4.5.1 Background	88
4.5.2 Bias-Enhanced H ₂ Plasma Pretreatment of Cr Film	89
4.5.3 Growth of Vertically Aligned Carbon Nanotubes	94
4.5.4 Field Emission Properties	100
4.6 Growth Model of Carbon Nanotubes by Using MPCVD	101
4.7 Comparisons between HWCVD and MPCVD	105
4.7.1 Deposition System	105
4.7.2 CNTs Characterization and Field Emission Properties	106
5 CONCLUSIONS AND SUGGESTIONS	109
5.1 Concluding Remarks	109
5.2 Suggestions for Further Study	112
REFERENCES	113
LIST OF PUBLICATIONS	127

List of Tables

Table 1	Isomers of carbon.....	5
Table 2	Mechanical Properties of CNTs compared with other Materials	13
Table 3	Metals and metal compounds catalysts for SWCNT synthesis.....	19
Table 4	Emission characteristics of CNT films.....	26
Table 5	Emission characteristics of CNT films studied under identical conditions.....	27
Table 6	Growth condition of HWCVD	38
Table 7	EDX analyses of metal catalysts in CNTs	80
Table 8	Comparisons between HWCVD and MPCVD deposition system.....	106
Table 9	Comparisons between characteristics and field emission properties of CNTs grown by using HWCVD and MPCVD	107



List of Figures

Fig. 1	Various forms of carbon: diamond, fullerene, graphite, and CNT	4
Fig. 2	C_{60} buckminsterfullerene	6
Fig. 3	Sketch illustrating the morphology of vapor grown carbon fibers	7
Fig. 4	Models of different CNT structures	8
Fig. 5	Schematic diagram showing how a hexagonal sheet of graphite is rolled to form a CNT	9
Fig. 6	TEM pictures of the ends of (a) a SWCNT, (b) a closed MWCNT, and (c) an open MWCNT. Each black line corresponds to one graphene sheet viewed edge-on	11
Fig. 7	Schematic illustration of the arc discharge system and TEM micrograph of the grown CNT	15
Fig. 8	Schematic illustration of the laser ablation apparatus	16
Fig. 9	Schematic illustration of the catalytic deposition and TEM micrograph of the grown CNT	17
Fig. 10	Carbon tube growth by precipitation from a seed metal particle. Gray circles with arrows are the thermal carbons from decomposition of hydrocarbons; filled circles are other atoms in the furnace volume	21
Fig. 11	Schematics of tip-growth and base-growth for carbon filament growth	21
Fig. 12	Diagram of the electron potential energy at the surface of metal	23
Fig. 13	CRTs and FEDs share many common features, including a glass vacuum envelope, and phosphor coated anode, and a cathode electron source	29
Fig. 14	Schematic structure of the matrix-addressed CNT display	30
Fig. 15	Samsung's 4.5 inch display	31

Fig. 16	(a) Cross-section of a CRT lighting element with a field emission cathode made of CNTs, and (b) photographs of CRT lighting elements emitting the three primary colors	32
Fig. 17	Comparing of dc breakdown voltage of a CNT-based GDT and commercial GDTs.....	34
Fig. 18	Schematic diagram of the direct HWCVD method	37
Fig. 19	Schematic diagram of the MPCVD system	39
Fig. 20	Schematic diagram of the I-V measurement.....	43
Fig. 21	SEM images of CNTs on silicon, obtained with 15 sccm CO ₂ carrier gas; (a) scale bar is 9 μm, and (b) scale bar is 600 nm.....	45
Fig. 22	TEM image of the multiwalled CNTs, obtained with 15 sccm CO ₂ carrier gas.....	46
Fig. 23	Micro-Raman spectrum of the CNTs grown on the silicon wafer.....	47
Fig. 24	SEM images of CNTs on silicon, obtained with CO ₂ carrier gas of various flow rate; (a) 15 sccm, (b) 45 sccm, and (c) 75 sccm	49
Fig. 25	SEM images of CNTs on silicon, obtained with Ar carrier gas of various flow rate; (a) 15 sccm, (b) 45 sccm, and (c) 75 sccm	50
Fig. 26	Micro-Raman spectra of the CNTs grown on the silicon wafer, obtained with CO ₂ carrier gas of various flow rate; (a) 15 sccm, (b) 45 sccm, and (c) 75 sccm	52
Fig. 27	Micro-Raman spectra of the CNTs grown on the silicon wafer, obtained with Ar carrier gas of various flow rate; (a) 15 sccm, (b) 45 sccm, and (c) 75 sccm	53
Fig. 28	SEM images of CNTs on silicon samples. (a) is obtained with CO ₂ carrier gas that flows horizontally, and (b) is obtained with CO ₂ carrier gas that flows vertically, in this experiment, CO ₂ flow rate is constant on 15 sccm	55

Fig. 29	Micro-Raman spectrum of CNTs on silicon samples. (a) is obtained with CO ₂ carrier gas that flows horizontally, and (b) is obtained with CO ₂ carrier gas that flows vertically	56
Fig. 30	TEM image of CNT, obtained with CO ₂ carrier gas that flows horizontally. The arrows 1 indicates the aligned wall of CNT, and arrows 2 indicates the defective graphitic sheets	57
Fig. 31	TEM images of aligned CNTs grown exhibit no bamboo-like structure; (a) scale bar is 20 nm, and (b) scale bar is 5 nm. The arrows 1 and 2 indicate the closed tips with no encapsulated metal particle	59
Fig. 32	Emission current density against applied voltage and the F-N plot of (a) random curved CNTs, and (b) aligned CNTs.....	61
Fig. 33	Metal elements profile of the wire and surface of the sample	63
Fig. 34	TEM image of CNT grown exhibit a bamboo-like structure. The arrow 1 indicates the closed tips with no encapsulated metal particle. The arrow 2 corresponds to the compartment layers whose curvature is directed to the tip.....	65
Fig. 35	(a) HRTEM image for the bamboo-like structure of CNT. The arrow 1 indicates the wall, the arrow 2 indicates the compartment layers, and the arrow 3 indicates defective graphitic sheets at the surface of wall. (b) Image indicates the open roots separated from catalyst particle	66
Fig. 36	Growth model of MWCNTs by using direct HWCVD.....	68
Fig. 37	SEM photographs of deposition product grown on stainless steel 304 at various biases for 10 min; (a) -300 V, (b) 0 V, and (c) +300 V.....	71
Fig. 38	Micro-Raman spectra of deposition product grown on stainless steel 304 at various biases for 10 min	72

Fig. 39	SEM photographs of CNTs grown on stainless steel 304 at a negative bias of -300 V for various periods; (a) 5 min, (b) 10 min, (c) 15 min, and (d) 30 min.....	73
Fig. 40	I_D/I_G ratio derived from Micro-Raman spectra of CNTs grown over various periods on stainless steel 304.....	74
Fig. 41	TEM image of the end section of CNTs grown on stainless steel 304 for 5 min.....	76
Fig. 42	TEM images of the carbon related nano-structure material grown on stainless steel 304 for 5 min; (a) scale bar is 50 nm, and (b) scale bar is 20 nm.....	76
Fig. 43	(a) TEM image of the end section of individual CNTs grown on stainless steel 304 for 30 min, and (b) EDX analysis of catalyst particle (Sample number 1).....	77
Fig. 44	(a) TEM image of the end section of individual CNTs grown on stainless steel 304 for 30 min, and (b) EDX analysis of catalyst particle (Sample number 2).....	78
Fig. 45	(a) TEM image of the end section of individual CNTs grown on stainless steel 304 for 30 min, and (b) EDX analysis of catalyst particle (Sample number 3).....	79
Fig. 46	Binary phase diagrams of C-Fe, C-Cr and C-Ni.....	81
Fig. 47	Emission current against applied voltage, and F-N plot of CNTs grown on stainless steel 304 at -300 V bias for 30 min.....	82
Fig. 48	SEM photographs of carbon grown on Cr film using the CH_4/CO_2 gas system at various biases; (a) No bias, (b) -150 V, and (c) -250 V.....	84
Fig. 49	Micro-Raman spectra of carbon grown on Cr film using the CH_4/CO_2 gas system at various biases; (a) No bias, (b) -150 V, and (c) -250 V.....	86

Fig. 50	(a) Relationship of emission current against applied voltage, and (b) F-N plot of the carbon nano-rods grown by using CH ₄ /CO ₂ gas system.....	87
Fig. 51	SEM photographs of bias-enhanced H ₂ plasma-pretreated Cr film, obtained for various periods of pretreatment; (a) 0 min, (b) 1 min, (c) 3 min, (d) 5 min, (e) 10 min, and (f) 30 min.....	90
Fig. 52	AFM images of bias-enhanced H ₂ plasma-pretreated Cr film, obtained for various periods of pretreatment; (a) 0 min, (b) 1 min, (c) 3 min, (d) 5 min, (e) 10 min, and (f) 30 min	92
Fig. 53	(a) Surface roughness, (b) average grain size and (c) particle size of H ₂ bias-enhanced plasma-pretreated Cr film, obtained for various periods of pretreatment	93
Fig. 54	SEM photographs of samples grown on H ₂ plasma-pretreated Cr film pretreated for various periods; (a) 3 min, (b) 5 min, and (c) 10 min.....	95
Fig. 55	Micro-Raman spectra of samples grown on H ₂ plasma-pretreated Cr film pretreated for various periods; (a) 3 min, (b) 5 min, and (c) 10 min.....	96
Fig. 56	SEM photographs of bias-enhanced H ₂ plasma-pretreated Cr film and resultant samples grown, obtained for various periods of pretreatment; (a) 3 min, (b) 5 min, and (c) 10 min	97
Fig. 57	TEM image of the end section of an individual CNT.....	98
Fig. 58	Emission current against applied voltage, and F-N plot for CNTs grown by using CH ₄ /H ₂ gas system	100
Fig. 59	TEM images of the CNTs grown on AISI 304 and Cr film by using MPCVD.....	102
Fig. 60	Growth model of CNTs by using MPCVD.....	104

Chapter 1 Introduction

Carbon nanotubes (CNTs), since their discovery in 1991 [1], have been considered for use in many different applications. The small dimensions, strength and remarkable physical properties of these materials make them the very promising emitters for field emission devices. Electron field emitters are now becoming increasingly attractive for flat panel displays. This resurgence is largely due to the recent development of cheap and robust field emitting materials. Although field emission devices based on microfabricated Mo tips are commercially available, researchers are actively looking for alternative materials. The ideal field emitter should be very long and very thin, made of conductive material with high mechanical strength, be robust, and cheap and easy to process [2]. CNTs show remarkable electronic [3-6] and mechanical [7-12] properties that have triggered an ever stronger effort towards applications. The power of CNTs as electron field emitters was already apparent from the first articles reporting extremely low turn-on fields and high current densities in 1995 [13-15]. Field emission devices based on CNTs have exhibited remarkable emission characteristics and good current stability [15,16], because of the high-aspect-ratio and electrical conductivity, as well as a mechanical stiffness of the CNTs [9,17]. This chapter introduces the motivation and outline of this study.

1.1 Background

Since CNTs were first observed by Iijima in 1991, various methods have been developed for their synthesis, including arc discharge [18], laser vaporization [19], pyrolysis [20], and chemical vapor deposition (CVD) [21-25]. Among these approaches, CVD methods hold some promise for scalability [24]; however, they require carefully prepared consumable substrate catalysts [22]. Thus, a low-cost CVD method which produces *in situ* catalysts for the growth of CNTs may be more valuable in practical applications. Several methods have been

reported for growing CNTs *in situ* without pre-deposition of a catalyst layer. One such method provides catalysts from the vapor source containing the metal element [26], while another uses the reactant gas which can act as a catalyst in certain substrates [27,28]. Furthermore, almost all methods use chemical means to produce a catalyst *in situ*; few employ physical vapor deposition, to produce such a catalyst. CNTs have been deposited as a by-product of diamond thick films in a hot filament CVD (HFCVD) system while copper was evaporated *in situ* from copper-covered parts near hot filaments to act as a catalyst during deposition [29]. However, this method seems to be an impractical means of synthesizing CNTs. Besides, the CNTs should have aligned vertically structure to apply in field emission.

1.2 Motivation and Objectives

In our previous studies [30-34], HFCVD and microwave plasma CVD (MPCVD) has been widely used for the growth of diamond film. Besides, good quality diamond was successfully synthesized by using MPCVD with CH₄/CO₂ gas mixture. The main purpose of this thesis is to provide a modified HFCVD method, hot wire CVD (HWCVD), to synthesis CNTs *in situ* without pre-deposition of a catalyst layer, and characterize the field emission properties. There are two reasons we rather the HWCVD than HFCVD. First, the word “filament” is also termed a carbon structure. Second, it may be misunderstood that filament is made up of tungsten as in bulbs. Furthermore, CNTs were grown *in situ* by MPCVD uses the reactant gas, CH₄/CO₂ gas mixture, in certain substrates. Finally, CNTs grown by these two methods were compared. Many studies have been conducted to achieve the goal. However, the following works will be more concerned:

1. To report a direct HWCVD method for preparing multi-walled nanotubes (MWCNTs) on silicon.
2. To synthesize aligned CNTs by MWCVD.
3. To developed the growth model of MWCNTs by direct HWCVD.

4. To study the bias effect, growth period, catalytic effect of CNTs grown on AISI 304 by MPCVD using CH₄/CO₂ gas mixture.
5. To synthesis CNTs on Cr film by MPCVD using CH₄/H₂ gas mixture.
6. To study the mechanism of aligned CNTs grown by MPCVD.
7. To understand field emission properties.
8. To compare HWCVD and MPCVD.

1.3 Outline of this Thesis

There are other four chapters in the thesis; a concisely summary of these chapters is as follows:

Chapter 2 Literature Review: The aim of this chapter is to provide a basic understanding about CNTs and the field emission. First, carbon materials, fullerence and carbon nanofiber, are introduced. Second, structures and properties of CNTs are focused. Third, synthesis methods of CNTs are interpreted. Finally, field emission theory and applications are presented.

Chapter 3 Experimental Details: Related deposition system and conditions of HWCVD and MPCVD are illustrated. The major analysis instruments used includes SEM, micro-Raman spectroscopy and HRTEM. Field emission properties were measured by a I-V measurement.

Chapter 4 Results and Discussion: There are seven subjects in this chapter. Research objectives listed above are interpreted, and the more concerned literature review is also discussed in this chapter.

Chapter 5 Conclusions and Suggestions: The results of the present investigation are summarized. On the other hand, some proposed relevant works are provided for further study.

Chapter 2 Literature Review

Through the achievements of the pioneers and other procedures, many research records about the CNTs applied in field emission can be found in a readable literature. In fact, there are many review paragraphs appeared in papers, reports, theses and CNTs handbooks. However, the aim of this chapter is to provide a basic understanding about the material aspect of CNTs, and the field emission related subject. Only some of the more basic literatures are discussed in this chapter. The more concerned literatures will be discussed directly in related objectives of Chapter 4.

2.1 Basic Knowledge of Carbon Materials

Carbon is the sixth element of the periodic table and is listed at the top of column IV. Carbon materials can be found in various forms as diamond, graphite, carbon fibers, fullerenes, and CNTs. Crystal structures of these carbon materials are shown schematically in Fig. 1. The reason why carbon assumes many structural forms is that a carbon atom can form several distinct types of valence bonds (or hybridization of orbitals).

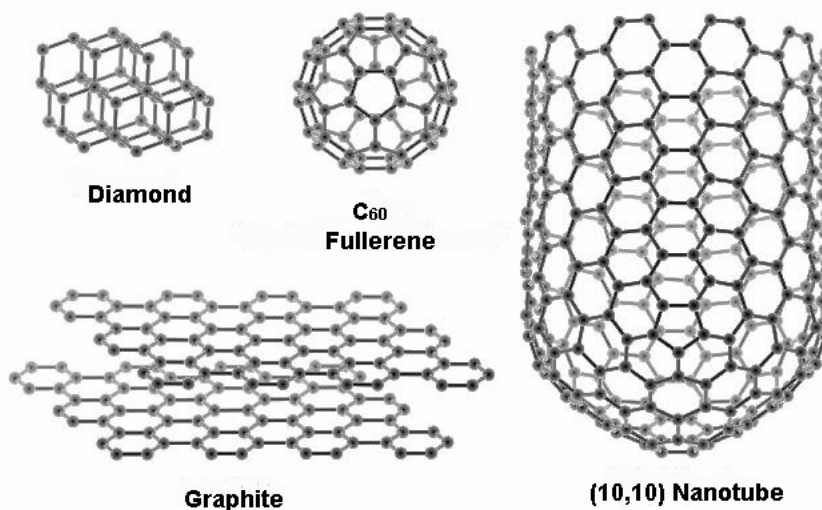


Fig. 1. Various forms of carbon: diamond, fullerene, graphite, and CNT [37].

Each carbon atom has six electrons $1s^2$, $2s^2$, and $2p^2$ theoretically. In carbon, there are three possible hybridized orbitals sp , sp^2 , and sp^3 . The sp^n hybridization is important for determining the dimensionality of carbon-based molecules and carbon-based solids. Carbon shows a variety of stable forms ranging from 0D fullerenes [35] to 1D conducting or semiconducting CNTs to 2D semi-metallic graphite to 3D semiconducting diamond, as shown in Table 1 [36]. In sp^n hybridization, $(n+1)$ σ bonds per carbon atom are formed. These σ bonds make a frame for the local structure of the n -dimensional structure.

Table 1 Isomers of carbon [36]

Dimension	0-D	1-D	2-D	3-D
Isomer	C_{60}	CNT	Graphite	Diamond
	Fullerene	Carbyne	Fiber	Amorphous
Hybridization	sp^2	sp^2 (sp)	sp^2	sp^3
Density [g / cm ³]	1.72	1.2-2.0	2.26	3.515
		2.68-3.13	~2	2-3
Bond Length [Å]	1.4 (C=C)	1.44 (C=C)	1.42 (C=C)	1.54 (C-C)
	1.46 (C-C)		1.44 (C=C)	
Electronic Properties	Semiconductor $E_g = 1.9$ eV	Metal or Semiconductor	Semimetal	Insulating $E_g = 5.47$ eV

In sp^3 hybridization, 4 σ bonds defining a regular tetrahedron are sufficient to form a 3D diamond structure. In sp^2 hybridization, it forms a planar structure in 2D graphite, and also forms a planar local structure in the closed polyhedron (0D) of fullerene and in the cylinders (1D) of CNT. Carbon fiber is macroscopic 1D material, because of the high length to diameter ratio. However, it consists of many graphitic planes and microscopically exhibits electronic properties that are mainly 2D. In sp hybridization, two σ bonds make only a 1D chain

structure, which is known as a carbyne. Besides, amorphous carbon is a disorder, 3D material in which both of sp^2 and sp^3 hybridization are present randomly. Amorphous graphite is the graphite with random stacking of graphitic layer segments, which consists mainly of sp^2 hybridization. Amorphous graphite can behave like a 2D material.

Next, fullerenes and carbon fibers, which are closely related to CNTs, are introduced. The main research object of this thesis, CNTs, is introduced apart in Section 2.2.

2.1.1 Fullerenes

Fullerene is an abbreviation of buckminsterfullerenes that honored the famous architect Buckminster Fuller, who designed and invented geodesic dome that was similar to the structure of C_{60} . In 1985, Kroto, Smalley, Curl and coworkers [38] began a famous series of experiments on the vaporization of graphite. In the distribution of gas-phase carbon clusters, C_{60} was the dominant species. This dominance became even more marked under conditions which maximized the amount of time the clusters were ‘annealed’ in the helium. Figure 2 shows C_{60} , which is a closed cluster containing precisely 60 carbon atoms would have a structure of unique stability and symmetry. The discovery of C_{60} marked the beginning of a new area in carbon science [39-42].

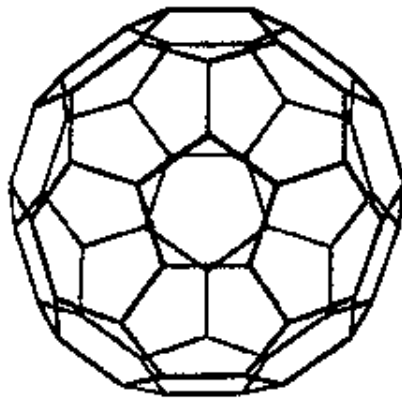


Fig. 2. C_{60} buckminsterfullerene [40].

2.1.2 Carbon Nanofibers

Carbon fibers represent an important class of graphite-related materials which are closely connected to CNTs, because of the high length to diameter ratio. Carbon fibers synthesized by traditional methods of extrusion from polymer slurries and from catalytic CVD vary in morphology and structure from fiber to fiber and area to area on each fiber. Despite the many precursors that can be used to synthesize carbon fibers, each having a different cross-sectional morphology, as shown in Fig. 3. Figure 3(a) shows carbon fibers as-deposited at 1100°C, and Fig. 3(b) shows carbon fibers which after treatment to 3000°C. The morphologies for commercial mesophase pitch fibers are shown in Fig. 3(c) for a “PAN-man” cross section with a radical arrangement of straight graphene ribbons and a missing wedge and Fig. 3(d) for a PAN-AM cross-sectional arrangement of graphene plane. A PAN fiber is shown in Fig. 3(e) with a circumferential arrangement of ribbons in the sheath region and a random structure in the core. The preferred orientation of the graphene planes is parallel to the fiber axis for all carbon fibers, thereby accounting for the high mechanical strength [43].

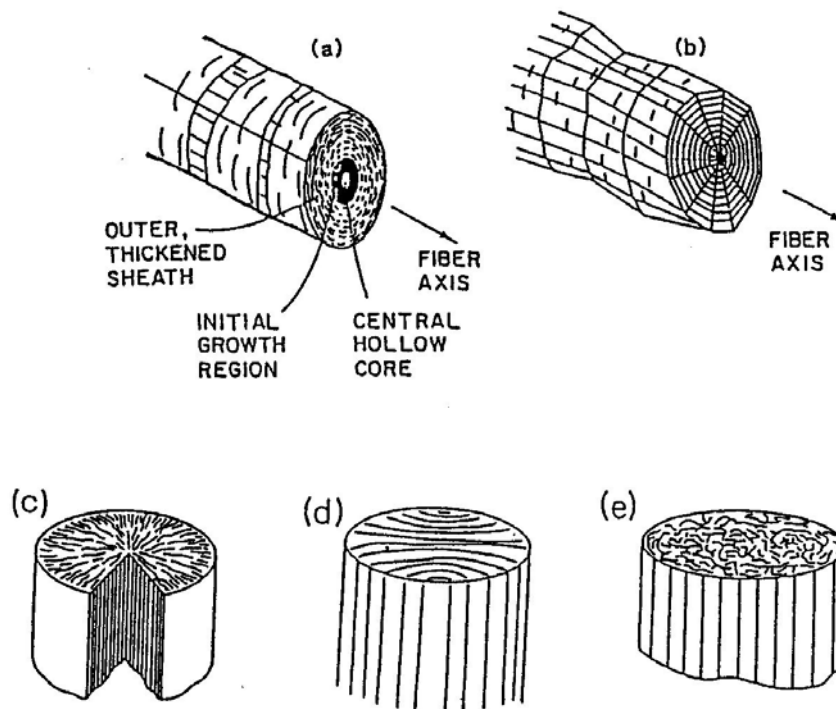


Fig. 3. Sketch illustrating the morphology of vapor grown carbon fibers [35].

2.2 Structure and Properties of Carbon Nanotubes

The main research object of this thesis, CNTs, is introduced here. Following paragraphs provide an overview of the structural and properties of CNTs, and there are many review articles [44-47] and books [35,48,49] surround this subject.

2.2.1 Structure

The detail structure of CNTs is discussed here. In the ideal case, a CNT consists of either one cylindrical graphene sheet (Single-walled nanotube, SWCNT) or of several nested cylinders with an inter-layer spacing of 0.34 - 0.36 nm that is close to the typical spacing of turbostratic graphite, i.e. MWCNT. There are many possibilities to form a cylinder with a graphene sheet [4] and a few configurations are shown in Fig. 4. Figure 4(a)-(c) are SWCNTs of (a) zig-zag, (b) armchair and (c) chiral type. Figure 4(d) represents a MWCNT formed by four tubes of increasing diameter with a layer spacing of 0.34 nm. One can roll up the sheet along one of the symmetry axis: this gives either a zig-zag tube, or an armchair tube. It is also possible to roll up the sheet in a direction that differs from a symmetry axis: one obtains a chiral CNT. Besides the chiral angle, the circumference of the cylinder can also be varied.

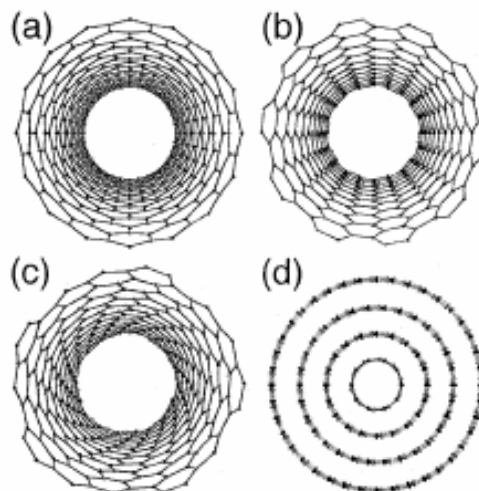


Fig. 4. Models of different CNT structures [2].

Figure 5 shows the cutting graphite sheet along the dotted lines which connects two crystalline graphite equivalent sites on a 2-D [50]. Each carbon atom has three nearest neighbors, rolling sheet of graphite into cylinder form CNTs. The circumference of CNTs can be expressed in term of the chiral vector, C_h , and chiral angle, θ . The chiral vector is given by Eq. (1):

$$C_h = na_1 + ma_2 \equiv (n, m) \quad (1)$$

(n, m are integers, $0 \leq |m| \leq n$),

where a_1 and a_2 are the primitive vectors length of which are both equal to $\sqrt{3} l_{C-C}$, with l_{C-C} is the length of C-C bond. The chiral angel determines the amount of twist in the tube. The chiral angles exist two limiting cases that are at 0° and 30° . The chiral angle is defined in Eq. (2) as

$$\cos \theta = \frac{C_h \cdot a_1}{|C_h| \cdot |a_1|} = \frac{2n + m}{2\sqrt{nm + m^2 + n^2}} \quad (2)$$

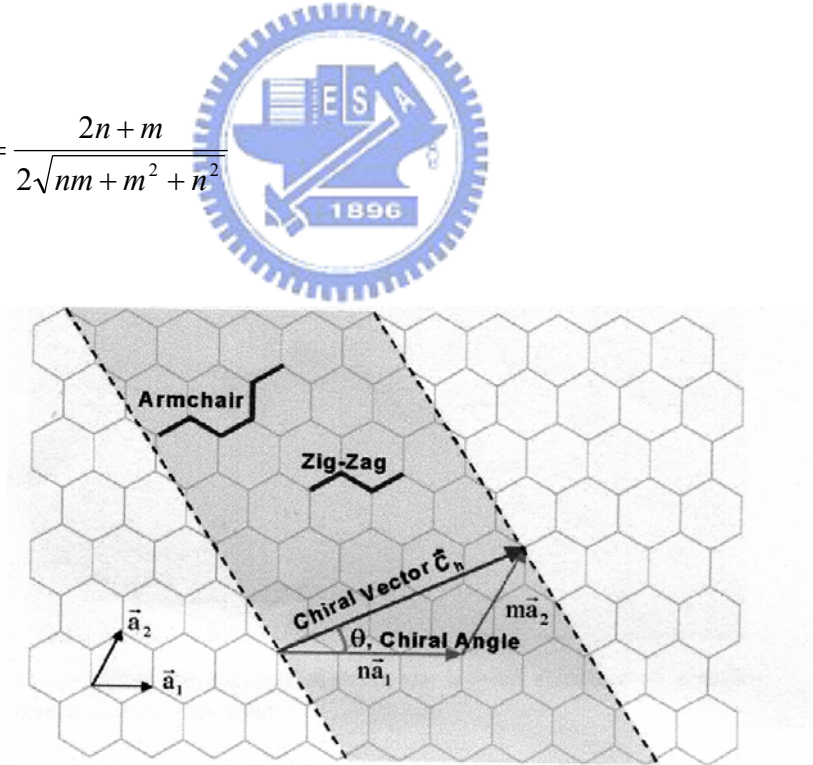


Fig. 5. Schematic diagram showing how a hexagonal sheet of graphite is rolled to form a CNT [50].

The zig-zag CNT corresponds to the case of $m = 0$, and the armchair CNT corresponds to the case of $n = m$. The chiral CNT corresponds to the other (n, m) chiral vectors. The zig-zag CNT $(n, 0)$ is generated from hexagon with $\theta = 0^\circ$, and armchair CNT (n, n) is formed from hexagon with $\theta = 30^\circ$. The chiral CNT is formed from hexagon with $0^\circ < \theta < 30^\circ$.

The inter-atomic spacing of carbon atom is known so that the rolled up vector of CNT can define the CNT diameter. The properties of carbon CNTs depend on the atomic arrangement, diameter, length, and the morphology [51].

This diversity of possible configurations is indeed found in practice, and no particular type is preferentially formed. In most cases, the layers of MWCNTs are chiral [1,52] and of different helicities [53]. The lengths of SWCNTs and MWCNTs are usually well over $1 \mu\text{m}$ and diameters range from $\sim 1 \text{ nm}$ (for SWCNTs) to $\sim 50 \text{ nm}$ (for MWCNTs). Pristine SWCNTs are usually closed at both ends by fullerene-like halvespheres that contain both pentagons and hexagons [4]. A SWCNT with a well-defined spherical tip is shown in Fig. 6. A MWCNT where the shape of the cap is more polyhedral than spherical is represented in Fig. 6(b). An open MWCNT where the ends of the graphene layers and the internal cavity of the tube are exposed is shown in Fig. 6(c). Defects in the hexagonal lattice are usually present in the form of pentagons and heptagons. Pentagons produce a positive curvature of the graphene layer and are mostly found at the cap as shown in Fig. 6(b) where each knick in the graphene layers points to the presence of pentagons in the carbon network. Heptagons give rise to a negative curvature of the tube wall [54]. Defects consisting of several pentagons and/or heptagons have also been observed. A simple model indicates that the diameter and/or chirality of the tube is changed from one side of the defect to the other [55]. Such an arrangement forms therefore a link between two different tubes and is accordingly called a junction.

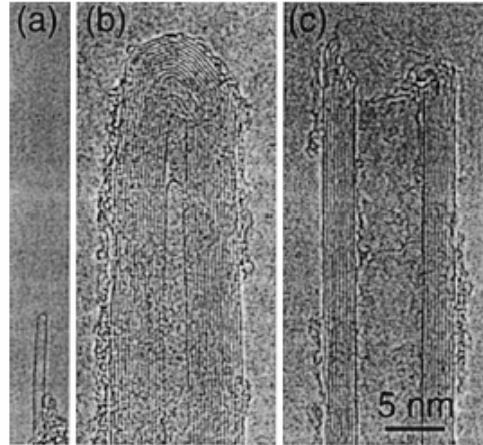


Fig. 6. TEM pictures of the ends of (a) a SWCNT, (b) a closed MWCNT, and (c) an open MWCNT. Each black line corresponds to one graphene sheet viewed edge-on [2].

2.2.2 Properties

This section is an overview of the mechanic and electronic properties of CNTs. The electronic properties of SWCNTs have been studied in a large number of theoretical works [3,4,56-58]. These models show that the electronic properties vary in a calculable way from metallic to semiconducting, depending on the tube chirality (n, m) given by [35]

Metallic properties: $n-m = 0$ or $(n-m)/3 = \text{integer}$

Semiconducting properties: $(n-m)/3 \neq \text{integer}$

The study shows that about 1/3 of SWCNTs are metallic, while the other 2/3 of SWCNT are semiconducting with a band gap inversely proportional to the tube diameter. This is due to the very unusual band structure of graphene and is absent in systems that can be described with usual free electron theory. Graphene is a zero-gap semiconductor with the energy bands of the p-electrons crossing the Fermi level at the edges of the Brillouin zone, leading to a Fermi surface made of six points [59]. Graphene should show a metallic behavior at room temperature since electrons can easily cross from the valence to the conduction band. However, it behaves as a semi-metal because the electronic density at the Fermi level is quite low [35,59]. Rolling up the graphene sheet into a cylinder imposes periodic boundary

conditions along the circumference and only a limited number of wave vectors are allowed in the direction perpendicular to the tube axis. When such wave vectors cross the edge of the Brillouin zone, and thus the Fermi surface, the CNT is metallic. This is the case for all armchair tubes and for one out of three zig-zag and chiral tubes. Otherwise, the band structure of the CNT shows a gap leading to semiconducting behavior, with a band gap that scales approximately with the inverse of the tube radius. Band gaps of 0.4-1 eV can be expected for SWCNTs (corresponding to diameters of 1.6-0.6 nm) [3,4,57]. This simple model does not take into account the curvature of the tube which induces hybridization effects for very small tubes [56] and generates a small band gap for most metallic tubes [58]. The exceptions are armchair tubes that remain metallic due to their high symmetry.

These theoretical predictions made in 1992 were confirmed in 1998 by scanning tunneling spectroscopy [5,6]. The scanning tunneling microscope has since then been used to image the atomic structure of SWCNTs [60,61], the electron wave function [62] and to characterize the band structure [61,63]. Numerous conductivity experiments on SWCNTs and MWCNTs yielded additional information [64-75]. At low temperatures, SWCNTs behave as coherent quantum wires where the conduction occurs through discrete electron states over large distances. Transport measurements revealed that metallic SWCNTs show extremely long coherence lengths [68,75,76]. MWCNTs show also these effects despite their larger diameter and multiple shells [77,78].

The fact that both MWCNT and SWCNT have indeed extraordinary mechanical properties has been indicated by a growing body of experimental evidence. Yakobson et al [79,80] inspected the instability of CNTs beyond linear response. Their simulation results show that CNTs are remarkably resilient, sustaining extreme strain with no signs of brittleness or plasticity. Besides, some experimental measures of the Young's modulus of CNTs have been reported. Treacy et al. [81] obtained a relation between amplitude of the tip oscillations and the Young's modulus. Through TEM observations of some CNTs, they defined the

amplitude of those oscillations and obtained an average value of 1.8 TPa for the Young's modulus. Another way to probe the mechanical properties of CNTs is to use the tip of AFM to bend anchored CNT. Young's modulus can be extracted while simultaneously recording the force exerted by the tube as a function of the displacement from its equilibrium position. By this way, Wong et al. [9] reported a mean value of 1.28 ± 0.59 TPa with no dependence on tube diameter for MWCNT. Walters et al. [82] investigated the elastic strain of CNTs bundles with the AFM. An experimental strain measurement and an elastic modulus of 1.25 TPa was assumed. Then yield strength of 45 ± 7 GPa was calculated.

Yu et al. [12,83] reported the tensile of SWCNTs and MWCNTs ropes. For MWCNTs ropes, the tensile strengths of the outermost layer ranged from 11 to 63 GPa and the elastic modulus ranged from 27 to 950 GPa. For SWCNT ropes, the tensile strengths in the range from 13 to 52 GPa and the average elastic modulus of 320 to 1470 GPa were obtained.

In term of mechanical properties, CNTs are among the strongest and most elastic materials known to exist in nature [84]. Table 2 shows the mechanical properties of CNTs with other materials. It indicates that MWCNTs are of the most superior mechanical characteristic. The hollow structure and close topology of CNTs form a distinct mechanical response in CNT compared to other graphitic structure.

Table 2 Mechanical properties of CNTs compared with other Materials [84]

Materials	Young's modulus (GPa)	Tensile strength (GPa)	Density (g/cm ³)
SWCNT	1054	~150	
MWCNT	1200	~150	2.6
(10,10) Nanorope	563	~75	1.3
Type I carbon fiber	350	2.5	2.6
Steel	208	0.4	7.8
Epoxy	3.5	0.05	1.25
Wood	16	0.08	0.6

2.3 Carbon Nanotube Synthesis

There are three major methods to synthesize CNTs: arc discharge, laser ablation and catalytically chemical vapor deposition.

2.3.1 Arc Discharge

The arc discharge was the first available method for the production of both MWCNTs [1,85] and SWCNTs [86,87]. This is the classic method of preparing MWCNTs, and produces the best quality samples. The method has been in use for a long time for the production of carbon fibers. Therefore, it is very possible that CNTs were observed but not recognized before Iijima observed CNTs synthesized from this method in 1991 [88,89].

Figure 7 shows the schematic of arc discharge system and TEM micrograph of the grown CNT [2]. The arc discharge apparatus involves the use of two graphite rods as the anode and cathode. The rods are brought together under a gas atmosphere (usually He, but H₂ [90] and Ar have also been used) and a voltage is applied until a stable arc is achieved. As the anode is consumed, a gap (~ 1mm) between cathode and anode is maintained by adjusting the position of anode. Carbon materials are deposited on the cathode to form CNTs and other carbon particles. MWCNTs produced by arc discharge are long and straight tubes closed at both ends with graphitic walls running parallel to the tube axis, as shown in Fig. 7.

Several factors have been shown to be important in producing a good yield of high quality of CNTs. Harris [91] reported that perhaps the most important is the pressure of the helium in the chamber, as demonstrated by Ebbesen and Ajayan [85]. The Current in the arc discharge method is another important factor [92,93]. Efficient cooling of the electrodes and the chambers has also been shown to be essential in producing good quality CNT samples [92-94].

To synthesize SWCNTs, Iijima et al. [86] and Bethune et al. [87] reported in 1993 that an arc discharge with a cathode containing metal catalysts (such as cobalt, iron or nickel) mixed

to graphite powder results in a deposit containing SWCNTs. The yield has been significantly increased by optimizing the catalyst mixture [95] and the deposition conditions [96].

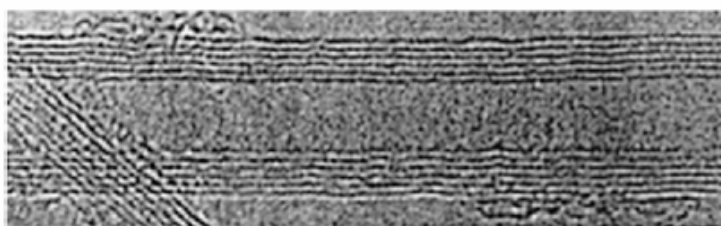
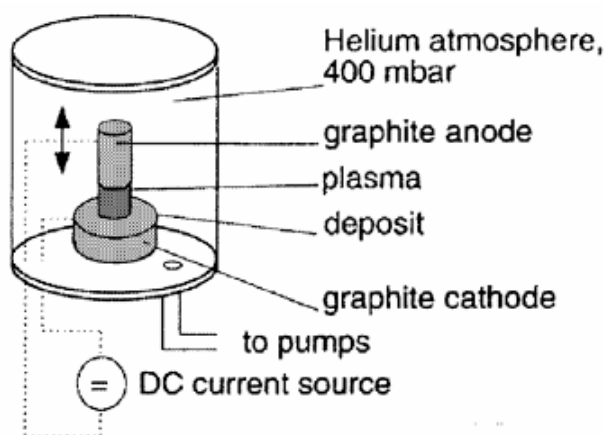


Fig. 7. Schematic illustration of the arc discharge system and TEM micrograph of the grown CNT. [2]

2.3.2 Laser Ablation

Laser ablation was first used for synthesis of C_{60} in 1985 by Kroto et al. [38], and was demonstrated to grow SWCNTs and MWCNTs in 1995 by Samlley's group at Rice University [19,97]. Subsequent refinements to this method led to the production of SWCNTs with unusually uniform diameter [98]. However, the length of MWCNTs grown by this method is much shorter than that by arc discharge method [19].

Thess et al. [98] showed that the synthesis could be carried out in a horizontal flow tube under a flow of inert gas at controlled pressure. In this setup the flow tube is heated to

~1200°C by a tube furnace as displayed in Fig. 8. Laser pulses enter the tube and strike a target consisting of a mixture of graphite and a metal catalyst such as Co or Ni. SWCNTs condense from the laser vaporization plume and are deposited on a collector outside the furnace zone [99]. The size of carbon sources limited the volume of sample. Besides, purification steps are necessary to separate the tube from undesirable by-product. Nevertheless, this method has still become an important technique for synthesizing SWCNTs due to the high yield of CNTs.

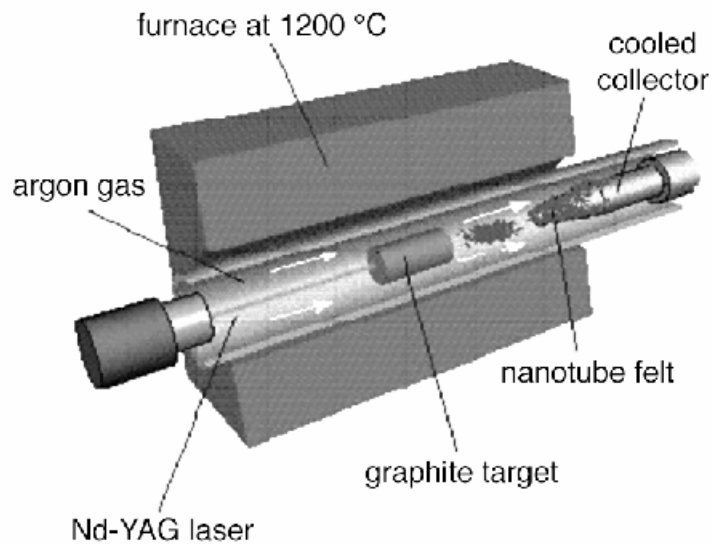


Fig. 8. Schematic illustration of the laser ablation apparatus [46].

2.3.3 Catalytically Chemical Vapor Deposition (CVD)

The catalytic growth of CNTs is an alternative to the arc discharge and laser ablation methods. It is based on the decomposition of the hydrocarbon gas over transition metals to grow CNTs by using chemical vapor deposition (CVD). Since the 1960s [100], carbon filaments and fibers have been produced by thermal decomposition of hydrocarbons. Usually, a catalyst is necessary to promote the growth [101]. A similar approach was used to grow MWCNTs from the decomposition of acetylene over iron particles in 1993 [102]. A tube

produced by catalytic growth is shown in Fig. 9. In general, the diameter of CNTs grown by catalytic growth is larger than that of arc discharge, but along with an imperfectly graphitized crystalline structure. To grow MWCNTs, acetylene is usually used as carbon source at temperatures typically between 600-800°C. To grow SWCNTs, the temperature has to be significantly higher (900-1200°C) due to the fact that they have a higher energy of formation. In this case carbon monoxide or methane must be used because of their increased stability at higher temperatures as compared to acetylene.

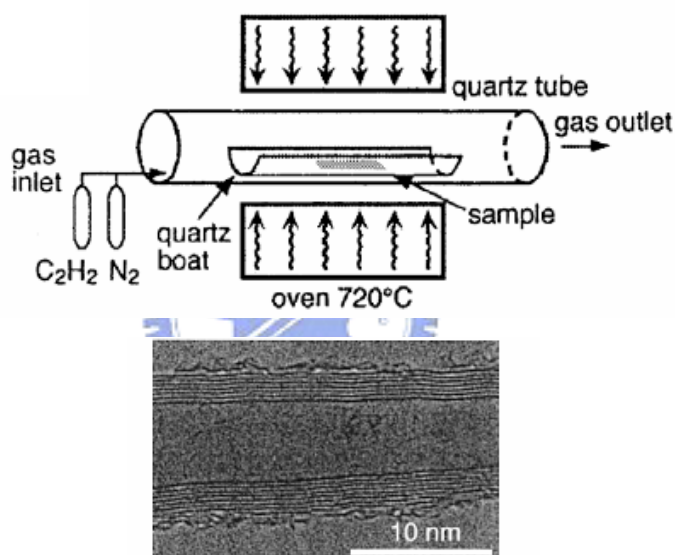


Fig. 9. Schematic illustration of the catalytic deposition and TEM micrograph of the grown CNT [2].

Up to now, the catalytic CVD has undergone many improvements. Co catalysts supported on silica particles produced straight as well as coiled MWCNTs [103], and the yield of CNTs was significantly increased by using zeolites as catalyst supports [104,105]. It was also reported that the continuous production of SWCNTs, where both the carbon and the catalyst are supplied in the gas phase. Besides, the yield and average diameter of SWCNTs could be varied by controlling the process parameters [106]. In addition, the type of catalyst

support was found to control the formation of individual or bundled SWCNTs [107]. Transition metal (e.g. Fe, Co, Ni) particles are known to be catalysts for vapor grown CNTs synthesis, in which hydrocarbons are used as carbon source. Metal catalysts are generally necessary to activate CNTs growth. A variety of other catalysts, hydrocarbons and catalyst supports have been used successfully by various groups the world wide to synthesize CNTs [108, 109]. Various metal compounds used as catalysts are listed in Table 3 [110]

The catalytic CVD is also an ideal method to grow CNTs on planar substrate (e.g. silicon or glass). Dense MWCNT arrays were thus deposited on mesoporous silica that was prepared by a sol-gel process [111] and long aligned CNTs were obtained over several square millimeters by using large-area mesoporous silica substrates [112]. Aligned MWCNTs were generated by pyrolysis of a triazine compound at 950°C with nearly no by-products [20]. There are some reasons behind the development of catalytic techniques to grow CNTs on planar substrates. First, in many cases, purification steps are unnecessary because there is no or very few by-product. Second, substrates can be directly patterned with catalysts using lithographic techniques followed by catalytic growth.

CNTs were also deposited by plasma-assisted CVD (PACVD) of methane and hydrogen at 950°C [113], and the synthesis temperature could be decreased below 660°C by using plasma-enhanced hot filament CVD [114]. Since then, several papers describing the synthesis of films of CNTs on silicon substrates have been published [22,115-117]. Moreover, microwave plasma-enhanced CVD of methane and hydrogen allowed to lower further the deposition temperature below 600°C on Ni-coated silicon [118], nickel [119], steel and Ni-coated glass [120] substrates. The synthesis of well-aligned CNTs on a variety of substrates was accomplished by the use of PACVD where the plasma is excited by a DC source [27] or a microwave source [28,121,122]. It was reported [114] that the ability to grow straight CNTs over a large area with uniformity in length, diameter, density, and straightness.

Table 3 Metals and metal compounds catalysts for SWCNT synthesis [110]

Metal/compound	Experimental conditions ¹	Locations of SWCNT ²	Density of SWCNT ³
Fe	Fullerence	Soot	High
		Extended deposition	High
Ni	Fullerence	Soot	High
		Extended deposition	High
Co	Fullerence	Soot	Low
		Tube	High
Fe/Ni	Fullerence	Soot	Very high
		Tube	Very high
Fe/Co	Fullerence	Soot	Low
		Tube	High
Ni/Co	Fullerence	Soot	Very high
		Tube	Very high
Ni/Cu	Tube	Soot	Low
		Soot	Very low
Cu/Co	Tube	Soot	Low
		Soot	Low
Y ₂ O ₃ /Co	Tube	Soot	Low, radial
		Soot	High, radial

¹ “Fullerence” for arc discharge at 100-Torr He and “Tube” at 550 Torr.

² “Soot” and “Extended deposit” protruding from the usual cathodic deposit, and “Weblike deposit”.

³ Categorized as very high, high, low and very low.

CVD technique deals with gas phase system in CNTs are formed by the deposition of carbon-containing gas [111]. The gas phase techniques are amenable to continuous process since the carbon source is continually replaced by flowing gas. In addition, the final purity of CNTs can be quite high enough to minimize purification steps. The advantage of CVD technique is that CNTs can be synthesized continually and thus the growing pure CNTs could be obtained in the optimum condition. That is a very good way to synthesize large quantities of CNTs under relatively controlled conditions. So the CVD has advantages for scale-up and commercial productions.

2.4 Catalytic Growth Mechanisms of Carbon Nanotubes

Many growth mechanisms have been proposed to explain the relation between the growth condition and the structure of CNTs. In this study, we focused on the mechanism in which the metal was used as catalyst. From many researchers' results, there may be more than one mechanism operating in the growth. Figure 10 shows a typical formation of the CNT in the present of a metal particle, which may include the following processes [48]:

1. Creation of a pure metal seed on a substrate;
2. Creation of a source of carbon atoms by the decomposition of hydrocarbons;
3. Condensation of carbons on the metal particle and nanotubes formation; and
4. Termination of the tube and closing (capping) the tube.

If the particles are considered to be spherical or pear shaped, the deposition of carbon atoms occurs on one half of the surface (on the lower curvature face for pear shapes). The carbon diffuses along the concentration gradient and precipitates on the opposite half, around and below the bisecting diameter. However, it does not precipitate from the apex of the hemisphere, which accounts for the hollow core that is characteristic of these filaments. Based on the position of metal particle on the filament, two kinds of growth mode were reported: 'base-growth' and 'tip-growth' [123]. The 'base-growth' mode means that the filament grows

upward from metal particles, which attach to the substrate. If the metal particles detach and move to the head of the growing filament, it is the ‘tip-growth’ mode. These mechanisms were illustrated graphically in Fig. 11 by Sinnott et al [124] (after Baker and Harris [123]).

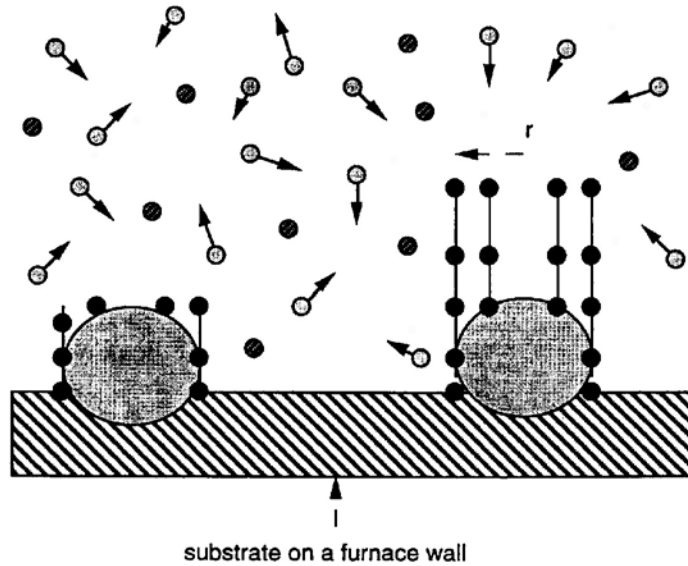


Fig. 10. Carbon tube growth by precipitation from a seed metal particle. Gray circles with arrows are the thermal carbons from decomposition of hydrocarbons; filled circles are other atoms in the furnace volume [48].

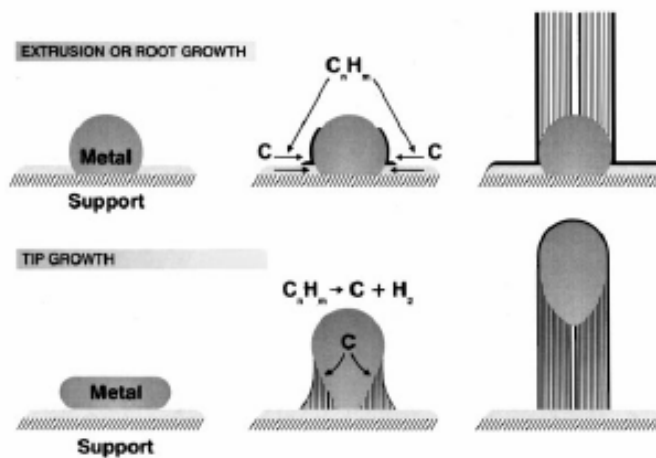


Fig. 11. Schematics of tip-growth and base-growth for carbon filament growth [124].

Andrews et al. suggested [125] that the catalyst particle size determines the size of the ‘filament’. When the particle diameter is in the range of tenths of a micron, the carbon is produced as filaments of similar diameter [123,126]. As the particle diameter is reduced, the filament curvature increases, imposing an increasing strain on the basal planes of the crystallites. Finally, a continuous surface is energetically more favorable and MWCNTs are formed.

2.5 Field Emission

The potential of CNTs for electron field emitters was already apparent from the first articles reporting extremely low turn-on fields and high current densities in 1995 [13-15]. CNTs can be used as electron sources in two different types of devices, i.e. single and multiple electron beam devices [2]. One possible application of a single electron beam instrument is an electron microscope that uses a single CNT as a field emission electron gun. In another way, flat panel displays are the most popular example of multiple beam instruments where a CNTs film provides a large number of independent electron beams. In this thesis, the field emission from CNT films is concerned.

2.5.1 Field Emission from Carbon Nanotube Films

Field emission is a quantum-mechanical phenomenon in which involves the extraction of electrons from a solid by tunneling through the surface potential barrier. Field emission is different from thermionic emission. In thermionic emission, electrons acquire sufficient energy through heating to overcome the potential barrier. In field emission, external electric fields are required for appreciable electron currents. The presence of the electric field makes the width of the potential barrier finite and therefore permeable to the electrons, as shown in Fig. 12.

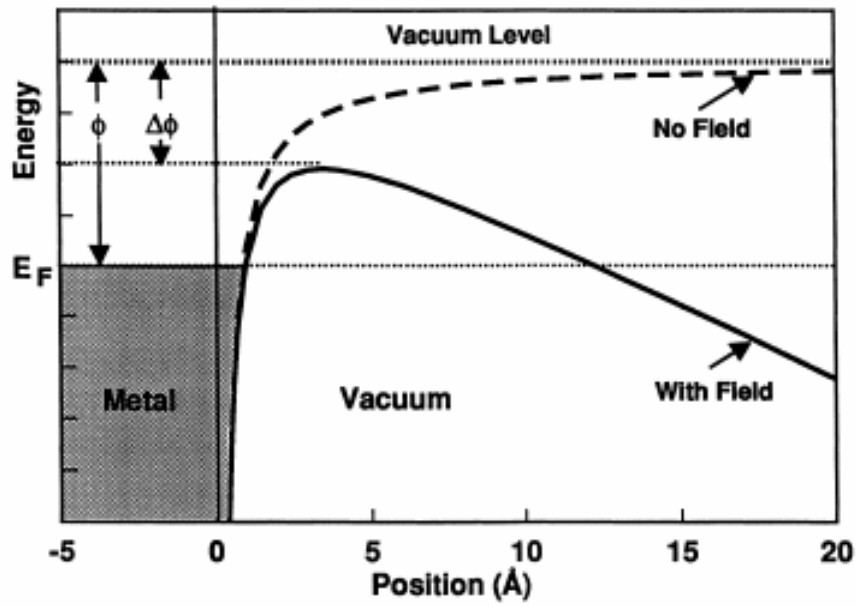


Fig. 12. Diagram of the electron potential energy at the surface of metal [127].

Figure 12 shows a diagram of the electron potential energy at the surface of metal. The dashed line shows the shape of the barrier in the absence of an external electric field. The height of the barrier is equal to the work function, ϕ , of the metal. The solid line corresponds to the shape of the barrier in the presence of the external electric field, E . The height of this barrier is smaller, with the lowering given by [128]

$$\Delta \phi = \left(\frac{eE}{4 \pi \epsilon_0} \right)^{1/2} \quad (1)$$

where e is the elementary charge and ϵ_0 is the permittivity of vacuum.

The probability of an electron with a given energy tunneling through the barrier can be calculated from the shape of the energy barrier. Integrating the probability function multiplied by an electron supply function in the available range of electron energies leads to an expression for the tunneling current density J as a function of the external electric field E . The tunneling current density can be expressed by Eq. (2) which is often referred to as the Fowler-Nordheim equation [129,130]

$$J = \frac{e^3 E^2}{8\pi h \phi t^2(y)} \exp\left[\frac{-8\pi(2m)^{1/2} \phi^{3/2}}{3heE} v(y)\right] \quad (2)$$

where $y = \Delta\phi/\phi$ with $\Delta\phi$ given by Eq. (1), h is the Planck's constant, m is the electron mass, and $t(y)$ and $v(y)$ are the Nordheim elliptic functions; to the first approximation $t^2(y) = 1.1$ and $v(y) = 0.95 - y^2$. Substituting these approximations in Eq. (2), together with Eq. (1) for y and values for the fundamental constants, one obtains [129]

$$J = 1.42 \times 10^{-6} \frac{E^2}{\phi} \exp\left(\frac{10.4}{\phi^{1/2}}\right) \exp\left(\frac{-6.44 \times 10^7 \phi^{3/2}}{E}\right) \quad (3)$$

where J is in units of A cm^{-2} , E is in units of V cm^{-1} and ϕ in units of eV. Plotting $\log(J/E^2)$ vs. $1/E$ results in a straight line with the slope proportional to the work function value, ϕ , to the 3/2 power. Although Eq. (3) applies strictly to temperature equal to 0 °K, the error involved in the use of the equation for moderate temperatures (~ 300 °K) is negligible [131].

From now on, one can find the emitted current depends directly on the local electric field at the emitting surface, E , and on its work function, ϕ . Besides, the Fowler-Nordheim model shows that the dependence of the emitted current on the local electric field and the work function is exponential-like. As a consequence, a small variation of the shape or surrounding of the emitter (geometric field enhancement) and/or the chemical state of the surface has a strong impact on the emitted current. These facts make a thorough comparison of results delicate, particularly because the methods used for synthesis (SWCNTs, MWCNTs), purification (closed or open ends, presence of contaminating material), and film deposition (alignment, spacing between the tubes) are very different. The interpretation is further complicated by the different experimental setups, e.g., the use of planar, spherical or sharp tip anodes, and different interelectrode distances. Finally, the film surfaces used for emission are in some cases quite small (below 10^{-4} cm^2). With such dimensions, one CNT emitting $10 \mu\text{A}$ is sufficient to yield an apparent current density of 0.1 A/cm^2 . Sufficiently large emission

surfaces ($>1 \text{ mm}^2$) have to be considered to ensure that the measurement is representative. We will therefore distinguish between integrated (or macroscopic) and microscopic emission to explain the large variation of observed current densities from micron- to millimeter-sized areas.

Most reports on the field emission present a typical I-V curve. Table 4 shows that field emission is excellent for nearly all types of CNTs. Typically, the turn-on fields are as low as $1 \text{ V}/\mu\text{m}$ and threshold fields around $5 \text{ V}/\mu\text{m}$. CNT films are capable of emitting current densities up to a few A/cm^2 at fields below $10 \text{ V}/\mu\text{m}$. One interesting parameter is the actual emitter density on the films. Usually, a film has a CNT density of 10^8 - 10^9 cm^{-2} . The effective number of emitting sites, however, is quite lower. Typical densities of 10^3 - 10^4 emitters/ cm^2 were reported at the onset of emission [15,16,132,133]. By using an optical microscope combined with a phosphor screen, Obraztsov et al. [134] were able to enhance the resolution of the measurement and reported densities of 10^7 - 10^8 cm^{-2} .

Table 4 reveals that the type of tubes has no absolute influence on the field emission. By discussing results acquired on different CNT films under the same experimental conditions, this point can be addressed in more detail. Table 5 summarizes some important parameters. This will clarify the influence of the different parameters on the field emission.

Table 5 reveals that several parameters have an impact on the field emission characteristics. The intrinsic structural and chemical properties of the individual tubes play a role, as apparent differences were found depending on the diameter [135] and surface treatment [136] as well as between closed and open tubes [135]. Besides, the density and orientation of the tubes on the film [135,137,138] influences also the emission.

Table 4 Emission characteristics of CNT films [2]

Emitter	d (μm)	S (cm^{-2})	E_{to} ($\text{V}/\mu\text{m}$)	E_{thr} ($\text{V}/\mu\text{m}$)	J_{max} (A cm^{-2})	Remarks
MWCNT	10-40	0.002	n.a.	<25*	1	Very dense “tubulene” film
MWCNT	15	0.003	n.a.	~15*	10	Very dense “tubulene” film
Arc MWCNT	20	0.008	n.a.	20*	0.1	
Arc MWCNT	30	0.007	4.0	6.5		
Arc MWCNT	125	0.07	2.6	4.6		
Arc MWCNT	125	0.07	1.1	2.2		Purified sample with closed caps
Arc MWCNT	20-100	2.5×10^{-5}	7.5*	10*	0.4	Open tubes dispersed in epoxy
Arc MWCNT	80	0.025	0.9*	4*		O ₂ plasma treated tubes dispersed in epoxy
Arc MWCNT	200	0.02	n.a.	1.5		Tubes dispersed in epoxy
SWCNT	125	0.07	1.5	3.9		
SWCNT	10-300	0.002	n.a.	4-7	4	
SWCNT	150	3.1	2.1*	n.a.		
CVD MWCNT	n.a.	0.001	1.7*	n.a.		
CVD MWCNT	70	n.a.	n.a.	4.8-6.1		Aligned MWCNTs, 15 emitters
CVD MWCNT	150	3.1	n.a.	2.1*		Large amount of graphitic fragments
CVD MWCNT	n.a.	0.0003	4.8	6.5	0.1-1	
CVD MWCNT	600	0.07	n.a.	≥ 5		
CVD MWCNT	150	0.2	3	6.6*		Si substrate
CVD MWCNT	500	0.1	1.6	5*		Steel substrate
CVD MWCNT	500	0.1	3	5.6*		Ni substrate
CVD MWCNT	10-300	0.002	0.75	1.6	1-3	Catalyst supplied in gas phase
Graphitic fibers	300	1-10	2.1	n.a.	0.2	

d is the interelectrode distance, S is the emission area, E_{to} and E_{thr} are the turn-on and threshold fields needed to produce an integrated current density of $10 \mu\text{A}/\text{cm}^2$ and $10 \text{mA}/\text{cm}^2$, and J_{max} is the maximal current obtained without destruction of the emitter. * indicates that the value was estimated or extrapolated from the presented data.

Table 5 Emission characteristics of CNT films studied under identical conditions [2]

Influence	Emitter	d (μm)	S (cm^{-2})	E_{to} ($\text{V}/\mu\text{m}$)	E_{thr} ($\text{V}/\mu\text{m}$)	Remarks
Density and geometry	MWCNT	25	n.a.	$< 2.7^*$	$\sim 4.8^*$	Random alignment
	MWCNT	25	n.a.	$\sim 40^*$	n.a.	Short vertical tubes
Geometry	Arc MWCNT	125	0.07	2.6	4.6	Average over 15 emitters
	SWCNT	125	0.07	2.8	5.2	Average over 12 emitters
	Open MWCNT	125	0.07	4.5	30	Average over 6 emitters
	Graphite fibers	125	0.07	5.6	14	Average over 5 emitters
Surface treatment	MWCNT ta-c coated	125-400	0.01	1.6	n.a.	
	MWCNT (as produced)	125-400	0.01	2.4	n.a.	
Density and geometry	SWCNT	10-500	10^{-5}	n.a.	2.4	Randomly aligned
	CVD MWCNT	10-500	10^{-5}	n.a.	3.5	Dense aligned arrays
Density	CVD MWCNT	125	0.007	9.8	14.4	Low density
	CVD MWCNT	125	0.007	2.2	3.3	Medium density
	CVD MWCNT	125	0.007	3.6	5.3	High density

The symbols are the same as in Table 4.

Bonard et al. [139] discussed the influence of the density on the macroscopic field emission. A study of the patterns revealed that the density and length of tubes were the only two parameters which changed from sample to sample. The films of medium densities with CNTs protruding over the film surface show emission at the lowest fields [139]. Furthermore, more clues were gained by characterizing the emission on a microscopic scale. A vacuum FE

apparatus was used to locally resolve field emission using a scanning tip [140]. The low density sample shows a rather inhomogeneous emission pattern with very few sites emitting a low current. The medium CNTs density obtains a much more homogenous emission image. Finally, high CNTs density yields a result similar to the low density one, while with an emission intensity higher by a factor of 10. These results complete the macroscopic characterization. Thus, it can be understood that a film of low density and short tubes will be an inefficient cathode. The medium density films show a very homogeneous and strong emission with a large number of emitting sites. The high density films, however, show a decreased quality of the emission. The reason originates from the combination of two effects: the intertube distance and the number of emitters. When the intertube distance is large, the field amplification factor is determined only by the diameter and the height of the CNT. When the intertube is decreased, screening effects become significant. Since the number of emitters increases with decreasing intertube distance, there will be an optimum distance for a maximal emitted current density. The calculations show that this distance amounts to 1-2 times the tube height [140]. The height of the tubes over the substrate (or the average film surface) is surely another important parameter [140]. Therefore, the turn-on fields for low density films are high because there are few emitters with short heights. Conversely, the emission from high density films is more efficient but remains low because of screening effects between densely packed neighboring tubes and because of the small height of the tubes. There is an ideal compromise between these two extremes, where the length of the tubes and the distance between neighboring emitters are both sufficient to reach a high field amplification along with an emitter density that is high enough to ensure homogeneous emission at low voltages.

2.5.2 Field Emission Applications of Carbon Nanotube Films

Applications based on an assembly of CNTs films are discussed here. CNTs have been demonstrated to possess remarkable mechanical and electric properties for field emission application [15,48]. A powerful application of electronic emission sources can be expanded to flat panel display such as field emission display (FED). The application of CNTs to FEDs requires their vertical alignment on cathode electrodes for better emission. In FED, electrons coming from millions of tiny emitters pass through gates and excite phosphor to light up pixels on the screen. This principle is similar to that of cathode ray tube (CRT) in television sets [141], as shown in Fig. 13. In a CRT electrons from a triad of thermionic emitters are scanned across the phosphor screen with electromagnetic deflection coils. In a FED electrons from an addressable array of cold cathode impinge onto a precisely aligned phosphor anode. Instead of just one gun spraying electrons, there are millions of emitters in FED. Because of the simpler assembly, custom performance and special sizes are less costly to produce. FED technology also offers many advantages including brightness, lightness and speed [141].

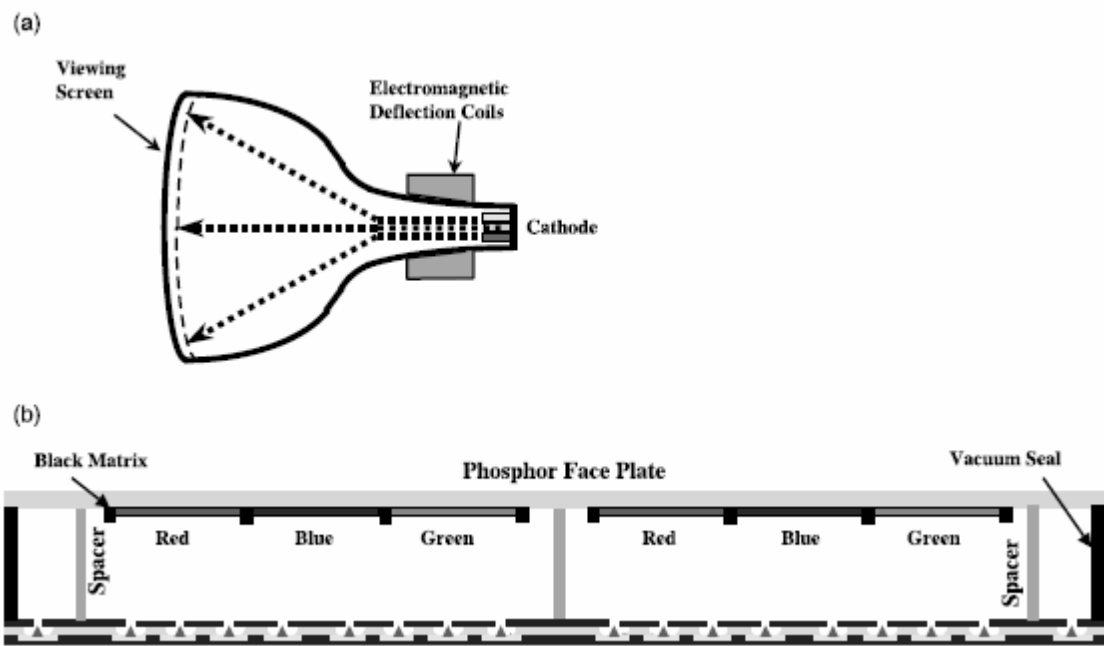


Fig. 13. CRTs and FEDs share many common features, including a glass vacuum envelope, and phosphor coated anode, and a cathode electron source [141].

CNT flat panel displays were proposed early on as a desirable alternative to other film emitters [13,15]. The first display with 32×32 matrix-addressable pixels in diode configuration has been fabricated using CNTs as the electron emission source by Wang et al. [142]. One demonstration structure constructed at Northwestern University consists of CNT-epoxy stripes on the cathode glass plate and phosphor-coated Indium-Tin-Oxide (ITO) stripes on the anode plate [142]. Pixels are formed at the intersection of cathode and anode stripes, as shown in Fig. 14. At a cathode-anode gap distance of $30 \mu\text{m}$, 230 V is required to obtain the emission current density necessary to drive the diode display ($\sim 76 \mu\text{mA}/\text{mm}^2$). The device is operated using the half-voltage off-pixel scheme. Pulses of $\pm 150 \text{ V}$ are switched among anode and cathode stripes, respectively to produce an image.

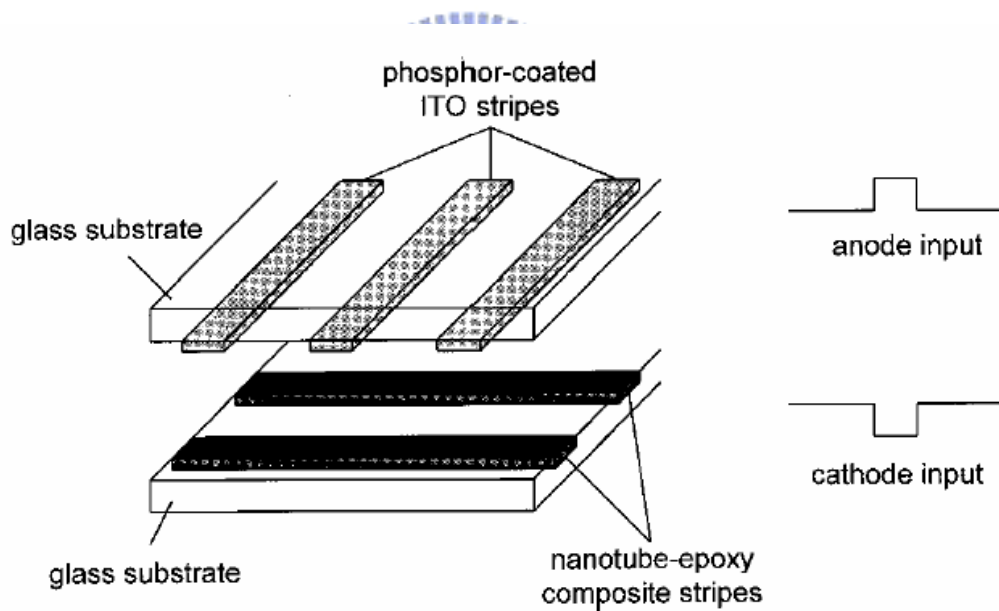


Fig. 14. Schematic structure of the matrix-addressed CNT display [142].

Recently, a fully sealed 4.5 inch three color field-emission display was demonstrated by Choi et al. [143,144], with SWCNT stripes on the cathode and phosphor-coated ITO stripes on the anode running orthogonally to the cathode stripes [143]. SWCNTs synthesized by the arc-discharge method were dispersed in isopropyl alcohol and then mixed with an organic

mixture of nitro cellulose. The paste was squeezed into sodalime glasses through a metal mesh, and then heat-treated to remove the organic binder. $Y_2O_2S:Eu$, $ZnS:Cu,Al$, and $ZnS:Ag,Cl$, phosphor-coated glass is used as the anode. This display has 128 addressable lines and works in diode configuration, as shown in Fig. 15. The emitting image of fully sealed SWCNT-FED at color mode with red, green, and blue phosphor columns. Since then, the Samsung research group has shown a 4.5 inch device displaying full-color images [145] and later a 9 inch full-color display with 576×242 pixels [146].

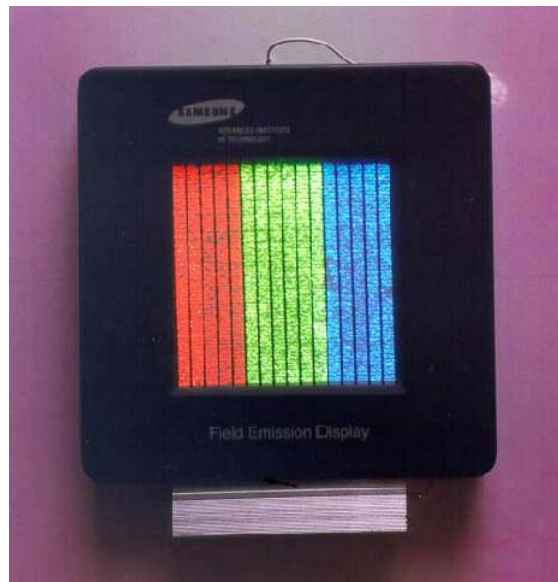


Fig. 15. Samsung's 4.5 inch display [143].

Cathode ray tube (CRT) with CNTs as the field emitters has been developed by Saito et al. and is reportedly commercially available [147]. These CNT-based lighting elements have a triode-type design, and light is produced by bombarding a phosphor-coated surface with electrons. Figure 16(a) shows the longitudinal cross-section of a CRT fluorescent display with a FE cathode made of CNTs. The outer diameter and the length of the glass bulb are 20 mm and 74 mm, respectively. Figure 16(b) shows photographs of CRT lighting elements emitting the three primary colors, green, red, and blue. Fluorescent materials are $ZnS:Cu, Al$

for green, $\text{Y}_2\text{O}_3:\text{Eu}$ for red, and $\text{ZnS}:\text{Ag}$ for blue. The anode currents and voltages are 200 mA and 10 kV, respectively [147]. In the early models, cylindrical rods containing MWCNTs, formed as a deposit by the arc-discharge method, were cut into thin disks and were glued to stainless steel plates by silver paste. In later models, CNTs are now screen-printed onto the metal plates. A phosphor screen is printed on the inner surfaces of a glass plate. Different colors are obtained by using different fluorescent materials. The brightness is typically higher by a factor of 2 as compared to conventional thermoionic CRT lighting elements operated under similar conditions and can be used for giant outdoor displays [148]. Lifetimes of 8000 h have been demonstrated with such devices [149]. Moreover, H. Murakami et al. suggests a lifetime of exceeding 10 000 h [120].

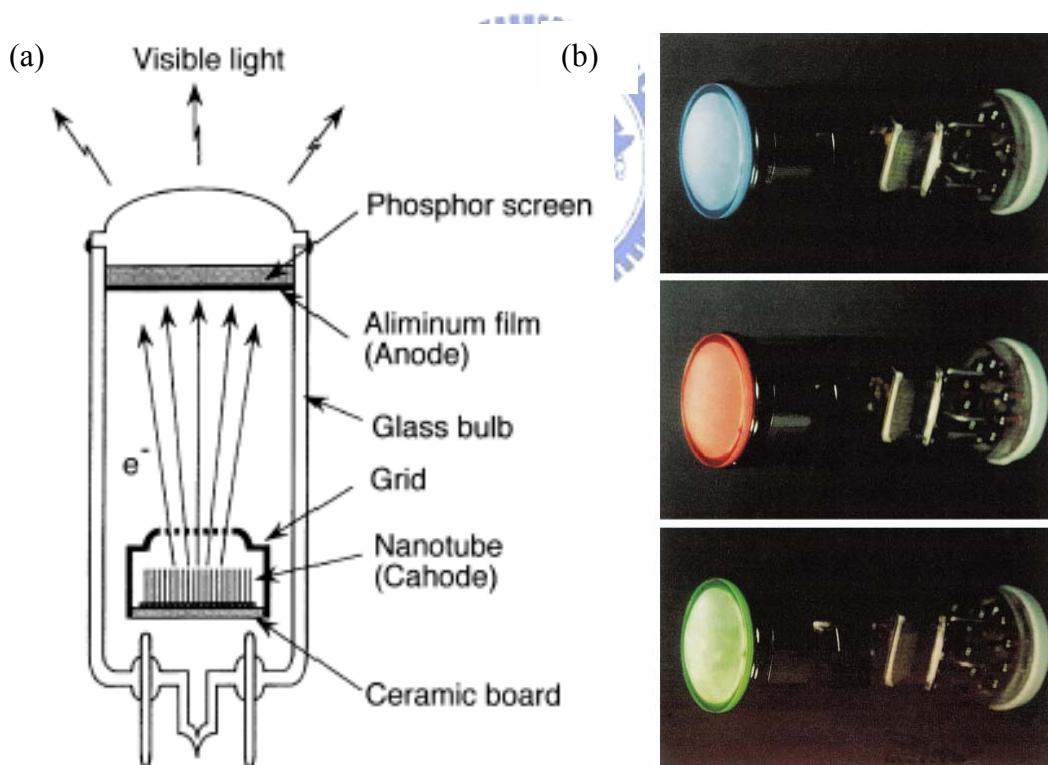


Fig. 16. (a) Cross-section of a CRT lighting element with a field emission cathode made of CNTs, and (b) photographs of CRT lighting elements emitting the three primary colors [147].

Field emitters are also of great interest for microwave amplification [150]. This type of application is very demanding because the current density must be at least 0.1 A/cm^2 . Zhou et al. constructed a prototype based on a SWCNT cathode that is able to reach that lower limit to operate in microwave tubes [151,152].

The same group realized a gas discharge tube (GDT) that serves as an overvoltage protection [153]. GDT protectors, usually consisting of two electrodes parallel to each other in a sealed ceramic case filled with a mixture of noble gases, is one of the oldest methods used to protect against transient over-voltages in a circuit [154]. They are widely used in telecom network interface devices boxes and central office switching gear to provide protection from lightning and ac power cross faults on the telecom network. They are designed to be insulating under normal voltage and current flow. Under large transient voltages, such as from lightning, a discharge is formed between the metal electrodes, creating a plasma breakdown of the noble gases inside the tube. In the plasma state, the gas tube becomes a conductor, essentially short-circuiting the system and thus protecting the electrical components from over-voltage damage. These devices are robust, moderately inexpensive, and have a relatively small shunt capacitance, so they do not limit the bandwidth of high- frequency circuits as much as other nonlinear shunt components. Compared to solid state protectors, GDTs can carry much higher currents. However, the current GDT protector units are unreliable from the standpoint of mean turn-on voltage and run-to-run variability.

Prototype GDT devices using CNT coated electrodes have recently been fabricated and tested by a group from UNC and Raychem Co. [153]. Molybdenum electrodes with various interlayer materials were coated with SWCNTs and analyzed for both electron field emission and discharge properties. Figure 17 shows dc breakdown voltage of a GDT with SWCNT/Fe/Mo electrodes, filled with 15 Torr argon with neon added and 1 mm distance between the electrodes. The commercial GDTs are off-the-shell products with unknown filling gases but the same electrode–electrode gap distances. The breakdown voltage of the

GDT with SWCNT/Fe/Mo electrodes is 448.5 V with a standard deviation of 4.8 V over 100 surges. The commercial GDT from manufacturer 1 has a mean breakdown voltage of 594 V and a standard deviation of 20 V. The GDT from manufacturer 2 has a breakdown voltage of 563 V and a standard deviation of 93 V. The breakdown reliability of CNT-based GDTs is a factor of 4-20 better and the breakdown voltage is ~30 % lower than the two commercial products measured. It could be demonstrated that this device shows better performance than commercially available elements.

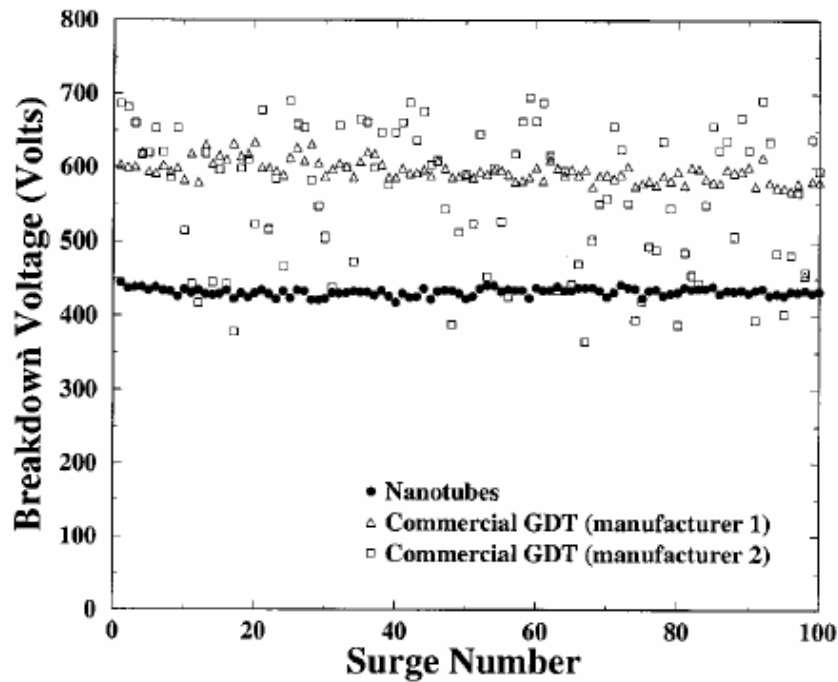


Fig. 17. Comparing of dc breakdown voltage of a CNT-based GDT and commercial GDTs [153].

In many field emission applications of CNTs, it is desirable to grow CNTs on cathode with well alignment for the reason of simplifying the process. Many researchers investigated the direct growth alignment CNTs methods which are compatible with current silicon

fabrication techniques for electronic application. Kind et al [117] synthesized well-aligned CNTs on Si wafer using microcontact printing of catalysts. However, it is still a challenge to directly fabricate the CNTs field emission for commercial application. Zhang et al. [155] investigated the fabrication of vertically aligned CNTs patterns by CVD for field emitters.



Chapter 3 Experimental Details

In this chapter, hot wire chemical vapor deposition (HWCVD) and microwave plasma chemical vapor deposition (MPCVD) methods used to grow carbon nanotubes are introduced. Besides, the methods to characterize the resultant carbon nanotubes are also interpreted.

3.1 HWCVD

3.1.1 Deposition System

A simplified CVD method for synthesizing nanotubes is described here. Figure 18 presents the schematic diagram of the direct HWCVD method. The proposed method eliminates nearly all of the complex and expensive machinery associated with conventional nanotube growth. This system consists of an ac transformer, an Fe-Cr wire as the filament, a gas flow meter, a container of alcohol, a substrate holder, and a quartz tube used as a reaction vessel. The synthesis apparatus is similar to that used to deposit CVD diamond. However, tungsten is the most commonly used filament material in diamond deposition. Here, an Fe-Cr wire is coiled as a filament to grow nanotubes and nanofibers. Such Fe-Cr wire is frequently used in furnace heating. The wire is not high-grade and has several impurities, being composed of Fe (71.4 wt %), Cr (22.5 wt %) and others. Deposition needed not be *in vacuo*, and process pressure was closed to the atmosphere.

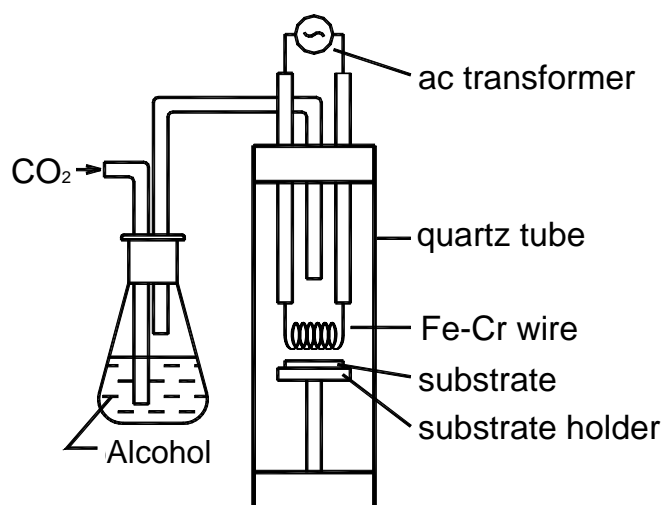


Fig. 18. Schematic diagram of the direct HWCVD method.

3.1.2 Depositing Conditions

Carbon nanotubes were deposited on the Si substrate with CO₂ or Ar as the carrier gas that passed through alcohol. Si substrates were mirror-polished p-type, (100)-oriented wafers with a resistivity of 1 - 10 Ω-cm. Silicon wafers were first sonicated in acetone, and then washed using DI water. Deposition is unnecessary *in vacuo*. The system used a 1-mm-diameter Fe-Cr wire, and was heated by an ac current of 22 A at 40 V. Different flow rate of carrier gases were adopted to confirm the effect of deposition conditions. While the flow rate of the carrier gas CO₂ was 15 sccm. The temperature of the Fe-Cr wire was approximately 1200 °C, which was 200 - 300 °C lower than its melting point. The distance of the wire to the sample was 2 mm. Different directions of flow of CO₂ onto the substrate were adopted to confirm the effect of deposition conditions by adjusting the position of the gas inlet nozzle. Growth was carried out for various durations, but it was found that growth for 15 min was sufficient to demonstrate the direct formation of CNTs on the surface of the silicon wafer. Table 6 lists the deposition condition of HWCVD.

Table 6 Growth condition of HWCVD

Wire	Fe-Cr wire
Carbon Source	Alcohol
Carrier Gas	CO ₂ or Ar
Flow Direction	Vertical or Horizontal
Pressure	~ 1 atm
Voltage	40 V (ac)
Current	22 A (ac)
Filament temperature	~ 1200 °C
Substrate temperature	~ 700 °C
Distance	2 mm
Growth time	15 min

3.2 MPCVD

3.2.1 Deposition System

Schematic diagram of the MPCVD system is shown in Fig. 19. A quartz tube attached vertically to the rectangular wave-guide was used as the deposition chamber. The microwave from a magnetron source (model IMG 2502-S, IDX Tokyo, Japan) was supplied to the quartz tube through an isolator, three-stub tuner, and a power meter. Next, the microwave power was coupled to the quartz tube through an aluminum wave-guide with a hole drilled through a top and bottom face. Aluminum tubes extend out from both holes; the tube extensions are water-cooled as well. A sliding short circuit was then attached at the end of the wave-guide. The lower position of the quartz tube was connected a stainless steel chamber that was equipped with a rotary pump. The substrates were positioned in the middle of the quartz tube waveguide intersection and held vertically by a substrate holder. The substrate holder of 20

mm diameter is made of molybdenum. Under the holder, it was attached to Ta wire which was connected to the bias system; it was used as the lower electrode in the bias treatment stage [156]. A quartz protector under the holder to protect the plasma was not attracted to the Ta wire attached to the Mo. The upper electrode, a Mo disk of 20 mm diameter, was placed 40 mm above the substrate; it was also attached to a Ta wire. The flow rate of the source gases was introduced into the chamber by mass flow controllers (model 647B, MKS instrument, Inc., USA) from the upper end of the quartz tube. An optical pyrometer was used to monitor the temperature of the plasma through a small window on the waveguide.

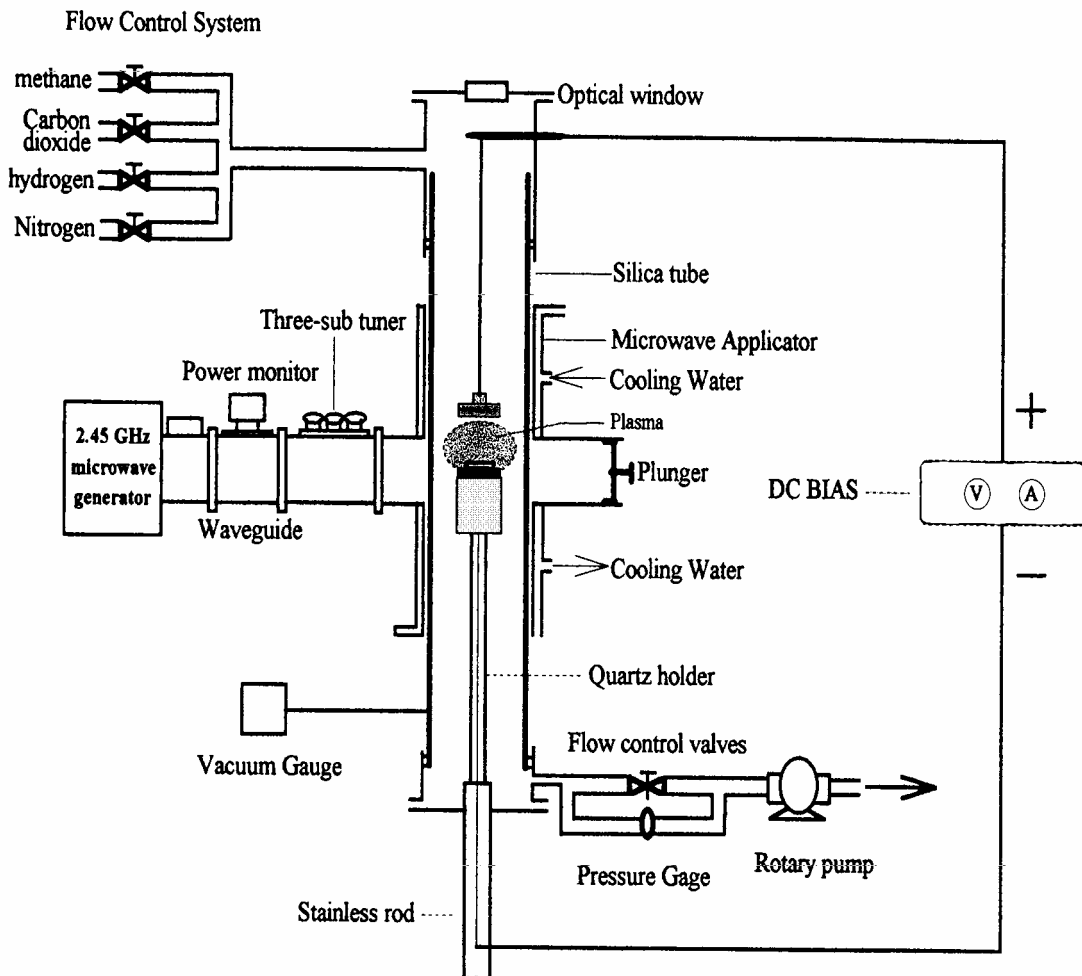


Fig. 19. Schematic diagram of the MPCVD system.

3.2.2 Carbon Nanotubes Grown on AISI 304

The stainless steel 304 had a thickness of 1 mm, and an area of 15 x 15 mm. Before deposition, samples were sonicated in acetone for 10 min, washed in DI water and dried using nitrogen gas. Bias-enhanced microwave plasma chemical vapor deposition was used to grow CNTs; various bias conditions and periods were used to grow the CNTs. The reactive gas mixture was CH₄/CO₂ at a flow rate of 30/22.5 sccm. The applied microwave power and pressure were 300 W and 1333 Pa, respectively. No bias, a negative bias voltage -300 V and a positive bias voltage 300 V were separately applied to the substrates to study the effect of the bias on the growth of CNTs on stainless steel 304. CNTs were grown at a bias of -300 V for various periods. An optical pyrometer was used to monitor the temperature of the substrate, which was maintained at approximately 600 °C.

3.2.3 Carbon Nanotubes Grown on Cr Film

The Cr film on a Si wafer had a constant thickness of 100 nm, and was coated on by DC sputtering. Before deposition, samples were sonicated in acetone for 10 min, washed with DI water and dried using nitrogen gas. In this study, the applied microwave power and the working pressure were 400 W and 2666 Pa, respectively. When CH₄/CO₂ was used, the reactive gas mixture was used directly with a flow rate of 30/30 sccm. The negative bias voltages applied to the substrates were 0 V, -150 V and -250 V. Since pure CO₂ plasma damaged the quartz tube in the deposition system, no pretreatment was performed during this experimental. However, when CH₄/H₂ was used, bias-enhanced H₂ plasma pretreatment was performed for various periods to modify the surface of the Cr film. During the Cr film pretreatment with H₂ plasma, the flow rate of H₂ was maintained at 300 sccm, and the negative bias voltage applied to the substrates was -150 V. During the growth of CNTs, microwave power, negative bias, and working pressure were not changed. The reactive gas mixture was CH₄/H₂ at a flow rate of 30/270 sccm. An optical pyrometer was used to monitor

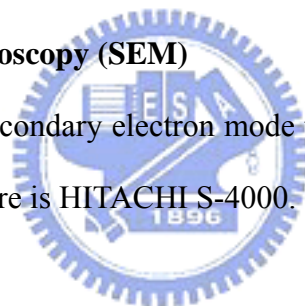
the substrate temperature, which was maintained at approximately 700 °C. In each case, growth continued for 30 min beyond the period of pretreatment.

3.3 Characterization of Carbon Nanotubes

A scanning electron microscope (SEM) was used to observe the original morphology and distribution of the CNTs. An atomic force microscope (AFM) was used to analyze surface roughness, grain size and particle size. A Renishaw micro-Raman spectroscope was used to characterize the CNTs' quality. Transmission electron microscope (TEM) was used to further characterize CNTs. The I-V measurement was used to analyze the field emission properties of the CNTs.

3.3.1 Scanning Electron Microscopy (SEM)

The SEM was used the secondary electron mode to observe the morphology of samples. The model of the SEM used here is HITACHI S-4000.



3.3.2 Micro-Raman Spectroscopy

Raman spectroscopy is an excellent technique for characterization of the CNTs. When photons illuminate a molecule or a crystal, they react with the atoms accompany with momentum change or energy exchange. Collecting the scatter photons, one can obtain a sequence of spectrum, including Raman scattering (Inelastic scattering) and Reyleigh scattering (Elastic scattering). The photon of Raman scattering can be classified into Stoke side and anti-Stoke side. Generally, Stoke side, which photons loss energy or the molecules gains energy, is used to characterize the material.

In this study, the CNTs' quality was analyzed by a Renishaw micro-Raman spectroscope (Model 2000). The laser light with the power of 200 mW was reflected by a half-mirror, and focused on to the sample with an objective lens. The spectral slit width is 0.4cm^{-1} .

3.3.3 Atomic Force Microscopy (AFM)

The AFM has proved to be one of the most exciting developments in surface science over the past decade. The AFM is a stylus-type instrument, in which a sharp probe, scanned raster-fashion across the sample, is employed to detect changes in surface structure on the atomic scale. The model of the AFM used here is Digital Instruments NanoScope II, and operated in tapping mode under ambient conditions. All images shown are the raw data; no filtering techniques have been employed.

3.3.4 High Resolution Transmission Electron Microscopy (HRTEM)

In this study, HRTEM (Tecnai 20, Philips) was used to further characterize CNTs. One of the typical characters of CNTs is their small size. Although some structural features can be revealed by x-ray and neutron diffraction, direct imaging of the CNTs is only possible using TEM. TEM is unique because it can provide a real space image on the atom distribution in the nano-crystal and on its surface. With a finely focused electron probe, the structural characteristic of a single CNT can be fully characterized. Besides, the energy dispersive X-ray spectroscopy (EDX) attached on TEM system was used to characterize the chemical components of catalyst particles in the CNTs.

3.3.5 I-V Measurement

Field emission properties are obtained using a diode structure. As shown in Fig. 20, an anode, made of indium tin oxide glass (ITO glass, MBC 6R1697), was separated by 500 μm from the tip of a cathode made of CNTs. The I-V properties were measured using an electrometer (Keithley SMU 237) in a vacuum of 1×10^{-6} Torr and analyzed using the Fowler-Nordheim (F-N) model. The anode-to-cathode voltage was varied from 0 to 1100 V. The turn-on and threshold field, defined respectively for 10 $\mu\text{A}/\text{cm}^2$ and 10 mA/cm^2 , have been used as the merit parameters to distinguish various emitter materials [2].

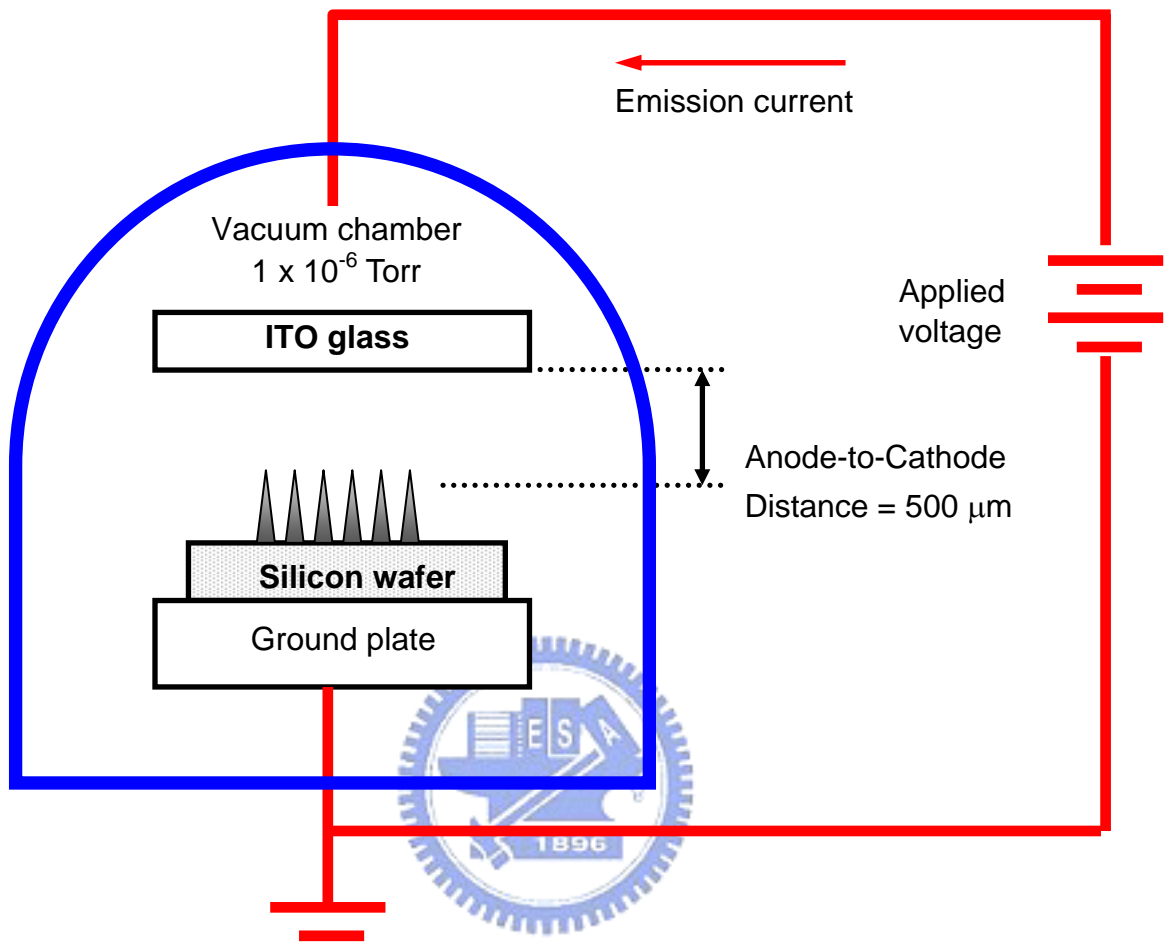


Fig. 20. Schematic diagram of the I-V measurement.